

Spaceborne multiband optical sensor for exoplanet detection onboard small satellite

Università degli studi di Napoli Federico II

Marcella Iuzzolino (PhD candidate),

D. Accardo (Academic tutor),

G. Rufino (Academic tutor)

2014-2017

Contents

1	Introduction	5
1.1	Exoplanets	6
1.2	Stars Classification	7
1.3	Exoplanets detection methods	9
2	Exoplanets Missions Overview	12
2.1	Existing Missions	12
2.2	Cubesat Missions	13
2.3	Methods to detect false alarms	15
3	Mission analysis	20
3.1	Why to go into space?	20
3.2	Mission Statement	21
3.3	Mission Objective	21
3.4	Methods comparison to detect exoplanets	22
3.5	Mission key concepts	25
3.6	Mission Analysis- Subsystems requirements	29
3.7	Mission Operation Concepts	31

3.8	Mission Data Flow Diagram	31
4	Orbit analysis	33
4.1	How to launch a cubesat?	33
4.2	Launch provider examples	35
4.3	Examples from other missions	36
4.4	De-orbiting	39
4.5	The orbit design process	39
4.6	Conclusion	45
5	Cubesat payload	46
5.1	Payload candidates description	46
5.1.1	Multispectral scanning solutions	46
5.1.2	Multispectral not-scanning solutions	47
5.2	The payload components	49
6	Cubesat architecture	57
6.1	The cubesat subsystems	57
6.2	Attitude determination and control subsystem	58
6.3	Communication Subsystem	59
6.4	Command and Data Handling	60
6.5	Thermal control subsystem	60
6.6	Electrical Power Subsystem	61
6.7	Structure Subsystem	66
7	Mission Target	71
7.1	Star visual magnitude limit	71

7.1.1	First postprocessing option	76
7.1.2	Second postprocessing option	76
7.2	Target Star	78
8	Payload functional simulation	83
9	Conclusion	87
9.1	Contributions	87
9.2	Future Work	88

Acknowledgements

I want to thank everyone that supported me in this hard parallel PhD work, from researchers to relatives, from recent friends to old friends, and a great thanks to everyone who make me stronger. Thanks.

Marcella

Chapter 1

Introduction

The search for undiscovered planets outside the solar system is a science topic that is rapidly spreading among the astrophysical and engineering communities. In this framework, the design of an innovative payload to detect exoplanets from a nano-sized space platform, like a 3U cubesat, is presented. The selected detection method is the photometric transit detection, and the payload aims to detect flux decrements down to $\approx 0.01\%$ with a precision of 12 ppm. The payload design is also aimed to false positive recognition. The suggested solution consists in a four-facets pyramid on the top of the payload, to allow for measurement redundancy and low resolution spectral dispersion of the star images. The mission innovative concept is the use of a small and cheap platform for a relevant astronomical mission. The faintest observable target star has V-magnitude equal to 3.38. Despite missions aimed at ultra-precise photometry from microsatellite (e.g. MOST, BRITe), the transit of exoplanets orbiting very bright stars has not yet been surveyed photometrically from space, since any observation from a small/medium sized (30

cm optical aperture) telescope would saturate the detector. This cubesat mission can provide these missing measurements. This work is set up as a demonstrator project to verify the feasibility of the payload concept.

In the following subchapters some basic background information is given about the exoplanets and astronomy science.

1.1 Exoplanets

An **exoplanet** is a planet that is orbiting around a star other than the Sun. A **terrestrial planet**, or 'rocky planet', has a surface defined by the extension of the liquid or solid interior, and is sustained by the gravitational collapse through the Coulomb pressure. The mass of this kind of planet should be less than 5-10 Earth masses, as larger planets are likely to capture gas during the accretion process and to become gas giants.

A **habitable planet** is a terrestrial planet with surface liquid water. To be detected life and water must be set on the planet surface, and this means that a planet atmosphere with a pressure and temperature suitable for liquid water is also needed.

A **potentially habitable planet** is a planet that orbits around its host star at a distance that lies in the habitable zone, and that also has a solid or liquid surface.

An **Earth-like planet** is a habitable planet of approximately 1 Earth mass and 1 Earth radius, and in an Earth-like orbit around a Sun-like star at a distance of roughly 1 AU.

An **Earth twin** is an Earth-like planet with liquid water oceans and con-

tinental land masses [1]. This project ultimate goal is to detect Earth-like planet, and thus the system requirements reported in next chapters concern this purpose.

1.2 Stars Classification

Star luminosity is the total amount of energy that a star emits per second. It is an intrinsic star property, and it is used to define the absolute magnitude of the star, that is the apparent magnitude of the star observed at the distance of 10 parsec.

Star flux is the energy amount per unit of time and area, and it is the physical quantity that we are able to observe and to detect with sensors. It depends from the observation distance from the star, and it has been used to experimentally define the apparent star magnitude.

The star spectrum signal is the star signature that identifies the chemical components of its atmosphere. According to their spectrum signal, stars are classified in spectral classes, that are: O, B, A, F, G, K, M. In this classification, also known as Harvard classification, each class is further divided in 10 subclasses, from 0 to 9. The mentioned class order is also a temperature classification, from the hottest bluish star to the coldest reddish one, assuming that the star emission is well approximated by the black body Wien's law.

Stars belonging to the same Harvard class, however, could show relevant differences in luminosity. A second classification system was then introduced by W. Morgan, P. Keenan and E. Kellman in 1943, also known as

MK classification. The classes are indicated by roman numbers. Through the Stephan-Boltzmann law, luminosity can be expressed as a function of the fourth power of the star surface temperature and the second power of the star radius. Hence stars belonging to the same spectral type could show different luminosities according to their radius.

In 1910/1913 two astronomers, Hertzsprung and Russell, identified the strong relation between the spectral type and the absolute magnitude of a star, as shown in the so-called H-R diagram.

The plot relates actually the star luminosity (from the absolute magnitude) to the star temperature (from the spectral type), and it shows that most of the stars lies in a diagonal stripe, the main sequence region, and they have a radius variation in a constrained range (from 0.1 solar radii to 20 solar radii). This most crowded region of the diagram is also the region where stars are located for the longest period of their lives, and thus there is a larger probability for us to observe them in the main sequence [2]. Stars belonging to that sequence goes from white or blue very bright stars of spectral type B and A, to stars of weak luminosity reddish color and M spectral type.

Another populated region of the H-R diagram is the horizontal branch, that includes very bright stars (10^2 Sun luminosity) of spectral type from F to M; these stars are called giant stars, while those belonging to the main sequence are called dwarfs.

The uppermost part of the H-R diagram includes the super giants stars, that show very high values of absolute magnitude.

Finally in the left-down corner there are the white dwarfs, that show low

luminosity and high temperature,[3].

The Sun is a G-type yellow dwarf main sequence star (G2V).

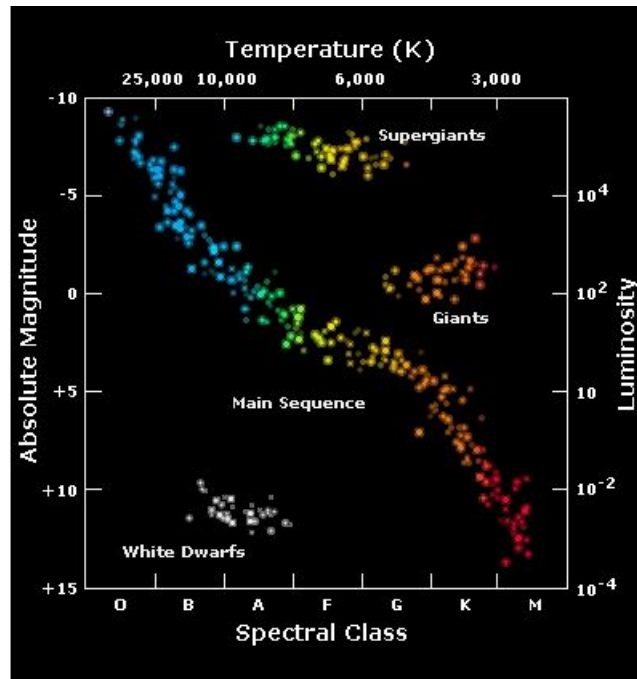


Figure 1.1: H-R diagram

1.3 Exoplanets detection methods

There are currently 6 detection techniques: radial velocity, astrometry, timing, gravitational microlensing, photometric transits, and direct imaging (see [1] for a detailed description).

The photometric transit technique consists in measuring the reduction of the star photometric flux when the planet passes in front of the host star as seen from the Earth.

The transit refers to a small body passing in front of a larger body, the occultation refers to larger bodies going in front of smaller bodies, and the eclipse refers to bodies of the same size passing one in front of the other [1].

This method is used both to observe new targets and to confirm targets that have already shown to be an exoplanet through the radial velocity method. In order to realistically observe the exoplanet transit, the exoplanet orbit around the host star must be aligned with the observer. From the transit detected in the star light curve it is possible to determine: the size of the planet compared to the size of the star, the orientation of the planet orbit, the presence of additional perturbing bodies of planets, and the characteristics of the atmosphere by further spectroscopic investigation. This method and the direct imaging method are the only ones that allow in principle to investigate also the planet's atmosphere.

By now (February 2017) the number of total confirmed exoplanets¹ is 3449. Among these the planets discovered by the photometric transit method are 2718², showing that this method is very effective. From 2718 planets, the number of terrestrial planets with planet mass between 0.6 Earth masses and 10 Earth masses, are 80³.

Since the signal decrement during the transit is proportional to the ratio between the planet radius and the star radius, it is more feasible to observe

¹(From <http://exoplanetarchive.ipac.caltech.edu/>. The criteria to list a exoplanet as a confirmed one are: the mass is equal or less than 30 Jupiter masses; the planet is associated with a host star (not a free floating); sufficient follow-up observations and validation have been undertaken to deem the possibility of the object being a false positive unlikely; the above information along with further orbital and/or physical properties are available in peer-reviewed publications.)

²(From <http://exoplanetarchive.ipac.caltech.edu/>.)

³(From <http://exoplanetarchive.ipac.caltech.edu/>.)

a transit around a star of V class, so this project is focused on dwarf stars belonging to the main sequence.

Chapter 2

Exoplanets Missions Overview

2.1 Existing Missions

The objective of detecting exoplanets transit is taking first place among the current astronomical space missions. In the following a brief list of the more relevant past/present/future missions regarding exoplanets transit detection, table 4.3.

CoRoT is the first mission ever designed to detect exoplanets transit from space, led by ESA and by CNES (Centre national d'études spatiales) from 2006 to 2013 [4]. The 27 cm diameter telescope observed in the band from 370 nm to 950 nm, and a one facet prism was installed before the CCDs used for transit detection [5].

Kepler is the NASA's first mission (from 2009 to 2013) able to find Earth-sized planets around Sun-like stars. The 0.95 m diameter telescope has a FOV (field of view) of 105 deg^2 , an array of 42 CCDs observing in the wave-

length band from 400 nm to 850 nm, with instrument relative precision of 10^{-5} . It continuously points at a single star field in the Cygnus-Lyra region, with a large number of stars but off the galactic plane to reduce field confusion [6].

TESS is the first spaceborne all-sky exoplanets transit survey from NASA-MIT (Massachusetts Institute of Technology), scheduled in 2017, observing in the band from 600 nm to 1000 nm [7].

CHEOPS is the first small class mission from ESA (European Space Agency), scheduled in 2017, to detect exoplanets transit on stars with visual V-magnitude between six and twelve anywhere in the sky, observing in the band from 0.4 to 1.1 μm [8].

PLATO is a medium class exoplanets transit detection mission from ESA (scheduled in 2025) in orbit around L2, looking at stars with a visual V-magnitude between 4 and 16 [9].

2.2 Cubesat Missions

There are also cubesat projects that aim at astronomical missions regarding exoplanets detection; a brief project list is provided in the following, table 4.2.

The most relevant cubesat project is the pioneer ExoplanetSat, a 3U cubesat from MIT and DraperLab. As a pathfinder mission, the mission objective is to detect exoplanets transit around bright stars with V-magnitude less than four. The key aspect of this project is a fine target pointing achieved by a closed control loop on the detector position to compensate for the satellite

jitter [10]. The project evolved in ASTERIA, a 6U cubesat with improved photometric capabilities.

MDOT is a 6U cubesat project from Stanford university in a HEO (High Earth Orbit) orbit. The project aims at taking a direct image of exo-zodiacal dust and transiting exoplanets using an occulter. The exo-zodiacal light is a portion of the star light that is scattered by the micrometric dust grains in the planetary system plane plus a dust thermal emission [11]. To detect the planet transit the central star light must be suppressed through the occulter. CANYVAL-X is a NASA mission and a formation flying demonstrator. The mission consists of 2U cubesat, used for the exoplanet detection, plus a 1U cubesat, used as occulter [12].

DeMi is a MIT study about a Cubesat Deformable Mirror Demonstrator in LEO (Low Earth Orbit) to enable space-based coronagraphic direct imaging of exoplanets from a 3U cubesat platform [13].

Centaur is a pathfinder mission to directly image exoplanets, using a new kilo-deformable mirror (1024 actuators), looking at Alpha Centauri AB.

PicSat is a 3U cubesat with the purpose of monitoring Beta Pictoris, a A6V star of $V = 3.86$ magnitude. The payload consists of a 35 mm effective aperture objective and a single pixel avalanche photodiode. A single-mode fiber guides the star from the focal plane to the photodiode. Like for ExoplanetSat project, a closed control loop is used to achieve a fine pointing [14].

2.3 Methods to detect false alarms

In a mission devoted to the exoplanet detection through the photometric transit there are several cases in which the target star brightness decreases for reasons other than a planet transit. The false positive signal sources belong to two possible groups: hardware faults and astronomical scenarios. The second group refers to astronomical objects other than planets that transit in front of the target star. The distinctive element of a planet transit is that the star light curve decreases uniformly in the entire visible band. Unlike the stars, the rocky planets temperature produces an approximately uniform spectral emission or absorption in the visible band. Moreover the target star intrinsic variability should also be taken into account [15].

The current approaches to discriminate the true signal from false positives are here briefly described.

Ground based complementary observations are often used to confirm a measurement, like photometry, high resolution spectroscopy, and radial velocity measurements [16].

Another strategy is to identify the pixel location of the transit signal with respect to the target pixel location. If the event is a false positive, the pixel location of transit signal does not coincide with the pixel location of the target flux. It works well just in cases of eclipsing object close enough to the observed target, so that the transit signal is not too much diffused [17].

A quite demanding strategy in terms of database size is the ephemerides matching, that consists in: first creating catalogs of transiting planets, eclipsing binaries, and other variable stars in the instrument field of view; secondly

defining a criterion to compare objects, according to their period and epochs; then looking for objects in the catalogs that fulfill the matching criterion according to their ephemerides. The found objects indicates at least one false positive event [17].

A more recent approach is the probabilistic method, that consists in computing the probability of the planet transit scenario against an exhaustive set of false positive scenarios. If the planet scenario is the highest probable one, then the planet is validated [16].

The estimated false detection rate of Kepler measurements, including the secondary eclipsing binaries, is of the order of 50 % (e.g. giant planet false positive rate indicated in [18]). Most of Kepler false positives are produced by background eclipsing binaries and planets transiting a star that is physically bound with the target star [16]. The false positive rate of CoRoT mission is 83%. In this mission the identification of false positives is realized only by the light-curves analysis, evaluating the transit depth and duration, the curve shape and the presence of color signature [19]. CoRoT astronomical field is denser than Kepler, so the probability to observe a false positive transit is higher. Moreover the CoRoT observation approach neglects the centroid follow up during the transit, i.e. measuring the centroid shift during the transit helps in rejecting possible background eclipsing binaries [16] [20]. However the main reason for this rate in CoRoT is the large PSF size of each star, such that the detector saturation was avoided, but the overlapping rate of stars PSFs was increased.

This project combines the growing interest for exoplanets search with the increasing success of cubesat platform. The project aims at detecting exo-

planets photometric transit, focusing on very bright stars, and discriminating a false positive detection.

Table 2.1: Medium and Large mission to detect exoplanets transits

Mission	Agency	Orbit	Wavelength band	Launch Mass	IFOV	Dates
CHEOPS	ESA	Sun-synchronous, 800 km, 6am-6pm	0.4-1.1 μm	250 kg	-	2017
Corot	ESA	Polar circular orbit, 896 km	0.37-0.95 μm	630 kg	2.7x3.05 deg	2006-2013
PLATO	ESA	L2	0.4-1.1 μm	M class	2250 deg ²	2025
TESS	NASA	High Earth Orbit	0.6- 1 μm	350 kg	576 deg ²	2017
Kepler	NASA	Earth- Trailing Heliocentric orbit	0.4-0.85 μm	1052 kg	105 deg ²	2009-2013

Table 2.2: Examples of cubesat scientific missions

Name	CANYVAL-X (NASA)
purpose	Exoplanet hunter with an occulter spacecraft Formation flying demonstrator
orbit	600km, 27.17 °
Deployer	P-POD (Falcon 9)
U	2+1 U

Name	MDOT (Stanford)
purpose	Direct imaging of exodial dust and exoplanets with occulter
orbit	HEO/GEO (with on-board thruster)
Deployer	-
U	6U

Name	ExoplanetSat
Purpose	exoplanets transits
Orbit	650 km, low inclination
Deployer	Elana-program
U	3U

Chapter 3

Mission analysis

3.1 Why to go into space?

There are two key aspects when observing an exoplanet transit from space. A space based observation ensures a high level of precision and consistency on the transit measurement, as required by the tiny flux decrement (0.01%) of a Sun-like star during the transit of an Earth sized planet [1]. The reason is that observations from space get rid of any atmosphere disturbance (seeing variations or scintillation) and limits, day-time cycle variation, moonlight, weather factors. A drawback of ground telescope observations is the limited scheduled observing time, while a space mission can be devoted even to the observation of a single target over the project lifespan. Even for ground-based instruments that are devoted to exoplanets research, the smallest detectable planets are Neptune's sized, i.e. mass near to 17.15 earth masses and radius near to 3.88 earth radii.

3.2 Mission Statement

The origin of this mission can be summarized in the following sentences, that represents the mission statements.

- Small satellites are a growing resource.
- Cubesat platform capabilities can be exploited for an astronomical mission.
- Exoplanets search is a present spread challenge.

3.3 Mission Objective

The project objective is to demonstrate the feasibility of a high performance astronomical mission with a low-cost space platform, and also to show a proof of concept about a valid technique against false positive signals.

The users are the astronomers that look for exoplanets, and the users need is to do exoplanets measurements in a easier/faster/and more reliable way.

The 'hidden objective' is to quickly provide a heritage in cubesat mission for exoplanets' detections, since no one has ever launched this kind of platform for this kind of mission.

3.4 Methods comparison to detect exoplanets

Radial Velocity

- Description: measurement of the star velocity along the line of sight between the star and the observer. It is more sensitive in selecting massive planets close to the star; it is able to push to low mass planets around bright stars
- Pro: the most mature technique
- Con: the orbital inclination is undetermined, and only a minimum mass of the planet is measured, $M_p \sin(i)$, where M_p is the planet mass and i is the orbit inclination.
- Need for a space mission: successfully done from Earth in the visible band and in the near infrared.

Astrometry

- Description: Star position measurements in the 2D sky plane.
- Pro: provide M_p (with no $\sin(i)$ uncertainty) and orbital elements.
- Con: small number of exoplanets discovered (none till 2010).
- Need for a space mission: the large mission GAIA is implementing this method.

Timing

- Description: measurement of time perturbations of stars with stable oscillation periods (e.g. pulsar stars, rotating neutron stars); infers planet presence

from star's orbital motion.

- Pro: extreme precision of the measurements. It is possible to detect planets with terrestrial mass as well as multiple planetary systems.
- Con: only planet mass and orbital elements can be derived. This method can be used only to observe pulsar stars, rare celestial objects that emit high energy radiation and prevent life formation.
- Need for a space mission: the first confirmed planet outside the Solar System regarded a planet orbiting a pulsar, and the used detection method was timing measurement from ground observation at the Arecibo radio telescope. Timing is a method successfully implemented by ground.

Gravitational microlensing

-Description: the foreground star (the lens) passes close to the observer's line of sight to a more distant background star (the source). The lens star magnifies the background star as a function of time, and the amount depends on the angular separation between the lens and the source star. If a planet orbits the lens star, it contributes in the magnification of the background star, and the light curve shows a peak that lasts several hours or days.

The microlensing effect consists in rays from the source star that are deflected by the lens star gravity. As the foreground star passes close to the line of sight to the background source, it splits the source into two images, which sweep out curved trajectories on the sky while the foreground star is moving. These two images are very little separated (1 mas) and are unresolved. The total area of these images is larger than the area of the source, and it exhibits a time-variable magnification, which is referred to as a microlensing event [1]. If the lens is exactly aligned with the source, it images the source

into an Einstein's ring [1].

- Pro: it determines the planet mass, orbit, period and the planet-star physical separation. It is able to detect the furthest and smallest planets, that orbit in moderate to large distances from their star. It is able to detect low-mass planets beyond the snow line. It is sensible to multiple planets systems. The microlensing signal can be detected also from other techniques measurements.
- Con: microlensing events are unique and do not repeat themselves. Distance of the detected planet from the Earth is known only by rough approximation
- Need for a space mission : It is a too rare event to test a cubesat platform.

Transits

- Description: the drop in brightness is indicative of the planet transit. It is often used to confirm targets already observed with radial velocity method. It requires alignment between planet orbit and star-observer line of sight.
- Con: The probability p to observe a transit is proportional to the ratio between the star radius and the planet orbit semi-major axis. It is easier to detect short period planets, that have a higher probability and have a more frequent transit, so the method is biased toward these kind of targets.
- Pro: from light curve it is possible to determine: planet size, star size, orbit orientation, possible perturbations due to multiple planets. The method allows also atmosphere investigation. It is the method with the biggest number of exoplanets detections, also thanks to Kepler mission).
- Need for a space mission: it is not possible to observe Earth sized transits from Earth, due to the excessive accuracy required.

Direct imaging

- Description: it is comparable to taking a snapshot of star and planet. The biggest challenge is to obscure the light scattered from the star, and to detect the planet image. Many new concepts of coronagraph have recently been introduced. Few attempts have been done related to spaceborne interferometric measurements from a satellites fleet, but no one have been accomplished, due to the high technical performance required.
- Con: To detect a exoplanets in a solar-system like it is required a solar-planet contrast of at least 5 orders of magnitude. The method is currently biased toward big massive objects and /or located far from the star.
- Pro: The method allows for both a photometric and spectral analysis, and provide accurate measurement of the orbit, and image of the circumstellar disk.
- Need for a space mission: This method requires the fulfillment of two high demanding technical challenges: the stabilization of the platform and the occultation of the star source.

3.5 Mission key concepts

The project key concepts are the followings.

1. Exoplanets detection (goal Earth-like planets around Sun-like stars)
2. Photometric transit method

3. Identification of false positive signals
4. 3U cubesat platform

Following a system engineering approach [21], each key concept defines a system driving requirement, who in turn determines one or more satellite subsystem requirements. The system driving requirements are shown below with the nomenclature $R.x$, where x is the key concept number.

$$\frac{F(t)}{F_s} \approx \left(\frac{R_{planet}}{R_{star}} \right)^2 \quad (3.1)$$

R.1 The amplitude of the signal to be detected is 84 ppm. During the transit the ratio between the combined flux from star and planet $F(t)$ and the unobstructed star flux F_s is approximated by the transit depth expression δ . The transit depth δ is proportional to the square ratio between the planet radius R_{planet} and the star radius R_{star} [1], equation 3.1 (neglecting at this time the influence of the star limb darkening on the transit depth). The assumed star is the Sun and the assumed planet is the Earth, table 3.1.

A central transit of an Earth-like planet lasts 13 hours. Considering that the cord length of a circle decreases as the cosine of the angle between the circle origin and the considered point on the circle, more than the 50 % of planet transits lasts 11.3 hours ($13 \cdot \cos(30^\circ)$), more than 70 % of planet transits lasts 9.2 hours, and more than the 86 % of planet transits lasts 6.5 hours. As a conservative choice, the assumed planet transit duration is 6.5 hours.

In this preliminary phase of the mission, the required signal to noise

Table 3.1: Expected transit depth of an Earth-like planet around a Sun-like star

Parameter	Value
R_{star} , Sun volumetric mean radius [km]	695700
R_{planet} , Earth volumetric mean radius [km]	6371
δ , transit depth	$84 \cdot 10^{-6}$

ratio is defined in analogy with Kepler mission. In that mission the detection threshold for the final S/N (a set of three or more transits) is 7.1σ [22], from the consideration of : the total number of independent tests for each star light curve, the total number of stars to be observed in the mission (10^5), and the requirement of one false alarm for the entire mission. In this cubesat mission the requirement of S/N equal to 84/12 is applied to each observation, for the duration of one duty cycle time, to be more conservative. This approach is also suitable to take into account further noise contribution not yet included in the noise budget (e.g. a thermal analysis will be included in the error budget, reducing the requirement margin). The duty cycle time derives from the orbit choice, and it is specified in the related paragraphs, Table 7.1.

The precision of the measurement requires a high pointing stability along the entire observation. As first choice (in analogy with ExoplanetSat example) the value of 5 arcsec is needed as pointing stability.

R.2 The required payload components are the objective and the detector

(photometric payload)

- R.3 To discriminate the false positive signal, the photometric signal is slightly dispersed. The observation band is the visible. The required spectral resolution is low (3 bands from 400 nm to 850 nm), since the measurement purpose is to monitor the centroid location of the dispersed signal.
- R.4 The standard cubesat structural limits in terms of dimensions and weight must be fulfilled. The 3U-cubesat dimensions are 10 cm x 10 cm x 30 cm (34 cm in 3U+ configuration) with a mass up to 4kg [23], figure 3.1. These small satellites require an orbital deployer (e.g. P-POD form CalPoly) to ensure that the cubesat is safely stored and correctly launched from the launcher. The advantage of choosing a cubesat platform is its straightforward design, realization, and test with a cheap budget. The drawbacks are the limited size and weight, and then limited resources for power, computing, and attitude control. The technical challenge is then to fulfill the mission objective through the limited capabilities of the cubesat space platform. Moreover the requirement of 3U size comes from the consideration that further mass increment (and thus unit increment, till about 8U) would not provide free space for an objective aperture wider than 100 mm (assuming to use a circular aperture shape). The minimum estimated size for the payload is 1 unit and at least 2 other units are required for the satellite subsystems. The number of 3 units is then considered the most suitable choice.

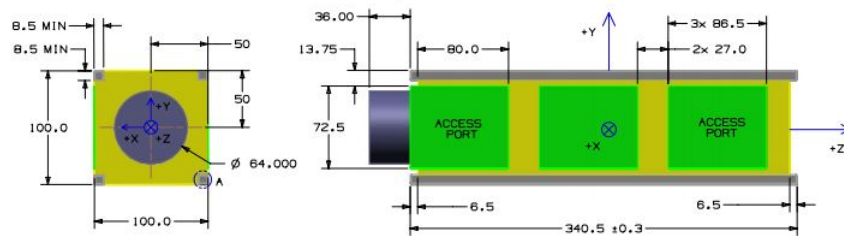


Figure 3.1: 3U+ standard configuration

3.6 Mission Analysis- Subsystems requirements

Cubesat Payload Subsystem

- R.1 The signal amplitude is 84 ppm, the tolerable noise level is 12 ppm in a duty cycle time observation. The detector resolution should fulfill the required dynamic range, and an intentional defocus can be introduced to enhance this range. A detector resolution equal or greater than 12 bit is suitable (see Mission Target chapter for more details).
- R.2 The payload is an instrument that provides photometric measurements working in the visible band, so the required components are at least: the optical system to focus the incoming light (a custom optics or a COTS objective suitable for space), and a detector. Signal detected through CMOS detectors are less affected by charges transfer errors induced by the radiation environment. Thus the first detector choice is CMOS oriented. The detector dynamic range is also a requirement to orient the choice between CCD and CMOS.
- R.3 The transit measurement signal must be redundant and spectrally dispersed. The observed star field should be uniformly and simultaneously

dispersed in the entire visible band.

R.4 The optical aperture diameter should be less than 10 cm. The payload subsystem should fit in 1 unit at maximum.

Cubesat Attitude Determination and Control

R.1 A pointing stability of 5 arcsec (first estimation) should be provided to detect the signal decrement.

R.4 The power consumption should be compliant with the total stored chemical energy, that can not exceed 100 Whr.

Cubesat Command and Data Handling

R.1 The onboard processing should be as limited as possible, to avoid any data alteration. The photometric measurement can be realized on a portion of the detector, in order to adjust the amount of data with the available data rate.

R.4 The power consumption should be compliant with the total stored chemical energy, that can not exceed 100 Whr.

Cubesat Structure and Mechanism

R.4 Platform dimensions are 10 cm x 10 cm x 34 cm. Platform maximum mass is 4 kg.

Mission Operation

R.1 The minimum mission lifetime is four years, to measure the transit of a exoplanet with a orbital period of one year at least three times.

The scientific operations consists in looking at one target star continuously during the cubesat orbital eclipse (duty cycle) to measure the star flux along the entire orbital period of the exoplanet.

3.7 Mission Operation Concepts

Starting from the cubesat deployment, the mission steps are described here in the following. Last three items define the typical phases in one cubesat orbit.

- Ejection from the deployer (e.g. P-POD)
- Solar array deployment
- De-tumble sequence
- Orienting the solar panel toward the Sun, using the Sun sensors
- Lost-in space algorithm using star tracker
- Observation of the target during orbital night
- Recharge of batteries during orbital day
- Ground station communication during orbital day

3.8 Mission Data Flow Diagram

As indicated in the figure 3.2 the data flow is developed in the following macro-steps.

Acquisition:

The detector acquires the star images. A selection of the detector focal plane is stored in the on board memory, waiting for the ground station in view. Attitude information relative to the time of acquisition are also stored, in order to match subsequent frames.

Transmission to the ground:

When in view, the ground station receives the scientific frame, and optionally a dark frame. On ground the scientific image is then calibrated.

Astronomers request:

Astronomers requests for the calibrated scientific image.

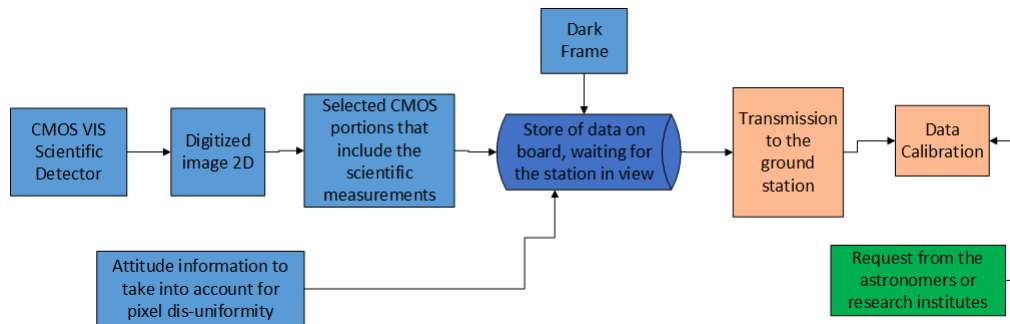


Figure 3.2: Data flow diagram

Chapter 4

Orbit analysis

4.1 How to launch a cubesat?

There is a growing number of private companies, whose core business is to provide cubesat orbital services.

The provided service consists in a launch opportunity from a Earth base site and in the cubesat insertion in orbit by the mean of a dedicated deployer structure, inside which the cubesat is tightly fitted.

The most famous cubesat deployer is the P-POD, Poly- Picosatellite Orbital Deployer, designed by the California Polytechnic State University (CalPoly). Nevertheless every private company usually develops its own cubesat deployer (e.g. GAUSS-POD, NanoRacks CubeSat Deployer NRCSD, ISIPOD cubesat deployer), in accordance with the cubesat standards.

The launch can take place as a piggyback launch, and the cubesat is the secondary payload of the launcher. Another option is to store the cubesat on a dedicated bigger satellite, the mother- satellite, usually owned by the

private company service supplier. In this case both piggyback and dedicated launch options are available for the mother-satellite. When in orbit, the mother-satellite deploys the cubesat(s) and inserts them in the designed orbit. Finally there is an increasing market trend of private companies trying to develop their own small launcher, devoted only to the launch of small/nano satellites (e.g. PLD, LEAFSPACE). this last one is a highly intriguing option, but it is currently work in progress, and thus can be considered only for future missions (at least 3 years from 2017).

The business interest for small satellites is spreading also in the field of launch sites. The Sweden Space Corporation SSC has started a project that consists in building a launch facility in ESRANGE space center (68°N 21°E north of Sweden), and cubesats are thought to be the typical satellite to be launched. The framework is the Rainbow project, that aims at achieving a European dedicated launch capability for small sats in ESRANGE. The cubesats would be launched in a sunsynchronous orbit at 500 km altitude, inclination of 97.4°, with ascending node local time selectable among 22:00, 06:00, 14:00, according to the mission requirements. The project was about to start the Phase B2 at the end of 2015 and it is foreseen to launch the first satellite in 2020 [24].

For educational activities there are also few European (QB50) and American (ELANA project) initiatives, that allow a easy and a cheaper way (even for free) to get the cubesat launched from the ISS.

4.2 Launch provider examples

GAUSS srl is a private company (spin-off from the Sapienza University). Its core business is related to the design and manufacturing of space systems both for cubesats and general small satellites platforms. GAUSS develops also a cubesat releasing platform, that is a small mother-satellite provided with GAUSS own cubesat deployer PEPPOD.

Two launch options are available from a GAUSS platform. The first launch option is through the DNEPR rocket, in collaboration with the International Space Company Kosmotras. The customer's cubesat gets onboard of a GAUSS mother-satellite, that is then picked up by the DNEPR rocket. The Gauss satellite is one of the Unisat family satellite built by the team with the explicit purpose of deploying cubesats in space and of providing also a customizable and completely controllable launch service, like cubesat launch 24 hours after the Unisat satellite in orbit injection. The planned orbit for the launch in December 2016 with Unisat 7 was Sun-Synchronous orbit, with altitude of 550 - 600 km, and local mean solar time of first ascending node of 10:30 [25].

The second launch option is onboard the ISS, thanks to the cooperation with JAMSS. The Japan Manned Space Systems Corp. (JAMSS) is the prime contractor to support JEM (Japanese Experiment Module, also known as KIBO, "hope" in Japanese) activities. Several launchers can be used to reach the ISS as a piggyback payload (e.g. HTV, ATV or SpaceX Dragon, H-IIA), and the KIBO module can release cubesats in orbit. The JAXA-developed cubesat deployer is J-SSOD, Jem Small Satellite Orbital Deployer, and it can deploy cubesats with a max dimension of 3U, and the typical deployment or-

Table 4.1: Launch provider orbit options

Company	Orbit Type	Altitude [km]	Inclination [deg]
SSC	Sun-synchronous	500	97.4
GAUSS	Sun-synchronous	550-600	98
GAUSS (ISS)	LEO	400	51.6
ISIS	custom	-	-

bit has 400 km altitude, inclination at 51.6° and orbiting life time of about 150-250 days [26].

Nanoracks is another private company that also provides the cubesat launch service from the Kibo module on the ISS.

ISIS is a private company specialized in the realization of small satellite sub-systems, such as radio-frequency systems and payloads, deployable systems and hold-down and release mechanisms, attitude determination systems, and embedded systems. It also offers regular piggyback launch opportunities for small spacecrafts to Low Earth Orbit on a variety of different launch vehicles. Different orbit types and specific launch periods may also be available on request.

A brief summary of the mentioned options is provided in table 4.1.

4.3 Examples from other missions

Example of orbit for cubesats missions (even not related to exoplanets detection) are listed in table 4.2, and example of orbit chosen by large and medium mission with the aim of detecting exoplanets is listed in table 4.3.

Table 4.2: Examples of Cubesat scientific missions

Name	Exocube (NASA)	Ceres (NASA)
Purpose	Space weather measurements	Radiation belt electron dynamics
Orbit	400km x 670km 98° i	High i, sun-synchronous LEO
Deployer	P-POD	P-POD
U number	3U	3U
Name	CANYVAL-X (NASA)	Picasso (ESA)
Purpose	Exoplanet hunter with an occulter spacecraft	Ozone and Ionosphere study
Orbit	600km, 27.17 °	550 km high inclination
Deployer	P-POD (Falcon 9)	ESA
U number	2+1 U	3U
Name	MDOT (Stanford)	SEAM
Purpose	Direct imaging of exodial dust and exoplanets with occulter	magnetic field measurements
Orbit	HEO/GEO (with on-board thruster)	600 km sunsynch.
Deployer	-	-
U number	6U	3U
Name	VZLUSAT-1	ExoplanetSat
Purpose	X-ray telescope	exoplanets transits
Orbit	400km LEO (QB50)	650 km, low inclination
Deployer	DNEPR + ISIS	Elana-program
U number	2U	3U

Table 4.3: Mission to detect exoplanets transits - orbit info

Mission	Orbit	Launch Mass	IFOV	Dates
CHEOPS	Sun-synchronous, 800 km, 6am-6pm	250 kg	-	2017
CoRoT	Polar circular orbit, 896 km	630 kg	2.7x3.05 deg	2006-2013
PLATO	L2	M class	2250 deg^2	2025
TESS	High Earth Orbit	350 kg	576 deg^2	2017
Kepler	Earth- Trailing Heliocentric orbit	1052 kg	105 deg^2	2009-2013

4.4 De-orbiting

The requirements concerning the space debris mitigation in the LEO region mandate that any space system that operates at an altitude below 2000 km should not interfere with the LEO region not later than 25 years after the end of the mission. For a cubesat design this requirement consists also in a constrain in terms of maximum orbital height (600 km for 3U cubesat) such that natural orbital decay is below 25 years. In general there is also the possibility to install on-board of the cubesat a system that accelerates the de-orbit phase, like drag increment system (e.g. clyde space AELODOS system), and as a result higher orbit becomes feasible (800km for 3U cubesat). Another alternative system can be a motor de-orbit system, e.g. ISIS Nanosatellite kick stage (1000 km 3U cubesat).

4.5 The orbit design process

The following design process originates from the SMAD book [21].

- Step 1 - Orbit types and functions

Parking orbits : not applicable;

Transfer Orbits: the mother-satellite (or the ISS module) injects the cubesat directly in the right orbit;

Space-referenced Orbit / Earth-referenced orbit : the cubesat operational orbit should allow the observation of the celestial target for a time as long as possible, and this becomes a requirement in terms of altitude and inclination. The chosen orbit must also ensure a good

communication with the ground station.

- Step 2 - Orbit related mission requirements

Accessibility

The orbit must be achievable by a cubesat launcher satellite. Change in orbit inclination would mean to have necessarily a propulsive system on-board, so this kind of orbit action is avoided.

Orbit decay rate and orbit stability

The orbit altitude should ensure the correct passive de-orbit in 25 years. The orbit altitude should be chosen in order to get a orbital decay rate due to atmospheric drag compatible with a mission lifetime of at least 4 years.

Radiation Environment

The orbit inclination should be chosen considering the radiation amount increment passing over the South Atlantic Anomaly and near the poles. The orbit inclination choice should contemplate that the more the Earth's magnetic field is uniform, the easier is the attitude control by the only mean of on-board magnetometers. The Earth's maximum magnetic field angular rate increases with lower altitudes and higher inclinations.

Ground Station communication

According to [21] it is possible to compute the percentage of coverage of a Earth latitude, in terms of fraction of orbits in a day or in terms of Earth's points percentage at that latitude. The starting data are orbit altitude, orbit inclination, and one parameter among the maximum spacecraft elevation angle ϵ , maximum nadir angle η , and the maximum Earth central angle, λ . This study requires to assume a ground station.

Orbital eclipse duration

It is convenient to compute the orbital eclipse duration (also refers to as duty cycle time of the observation) in the Spacecraft-Centered Celestial Sphere Earth-referenced coordinate system. The orbit plane is the equator, and the direction of the Earth is along the +X axis. This axis is always facing the Earth and this coordinate frame rotates once per orbit about the orbit pole. Also any object approximately fixed in the inertial space appears to rotate once per orbit around the orbit pole. In figure 4.1 the heavy solid line parallel to the equator represents the path followed by the Sun in one orbit, and an eclipse occurs when the path of the Sun goes behind the disk of the Earth. The angle β_S is the latitude of the Sun with respect to the equator of the coordinate system (i.e. the orbit plane), while β'_S is the co-latitude. The angle $\phi/2$ is half of the rotation angle corresponding to the eclipse duration (from the nadir to one side extreme position of the Sun during an eclipse), Figure 4.2.

The eclipse computation starts from the angular radius ρ of the Earth

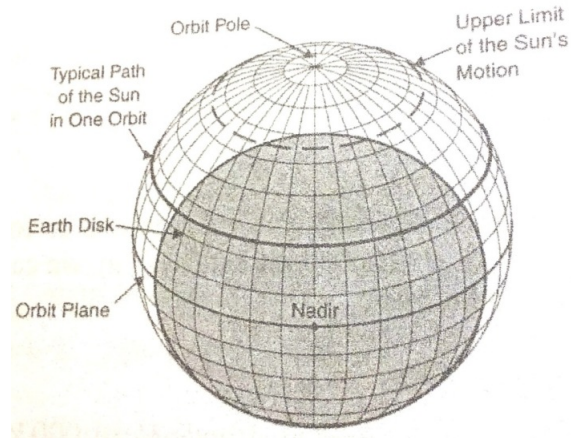


Figure 4.1: Spacecraft Centered Celestial Sphere, Earth referenced

as seen from the spacecraft, assuming a value for the orbit altitude. For an average eclipse duration the value for the angle β_S must be assumed less than its maximum value β_{Smax} , that is the sum of the orbit inclination plus the Earth axis inclination (about 23 deg). Most of the time the eclipse duration is close to its maximum value, so for an average analysis the value of β_S should be lower than the average between zero and β_{Smax} .

The ϕ angle, that is the angular eclipse duration, comes from the equation 4.1 . The orbital period in minutes is computed from equation 4.2, considering the orbit altitude and assuming a circular orbit. Then the eclipse duration (Eclipse Time in minutes, ET) is calculated from equation 4.3. The maximum eclipse duration occurs when the Sun is in the satellite orbital plane. As shown in the figures 4.3 and 4.4, the eclipse time decreases if the inclination increases for a fixed orbit al-

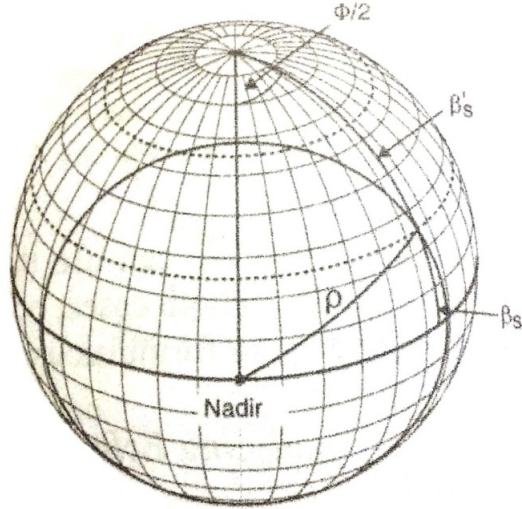


Figure 4.2: Eclipse Geometry Computation

altitude (600 km), and the eclipse time decreases as the orbit altitude increases for a fixed orbit inclination (11 deg). In the figure 4.4 the value for β_S is taken equal to half the maximum β_S .

$$\cos \phi/2 = \cos \rho / \cos \beta_S \quad (4.1)$$

$$P[min] = 1.659 \times 10^{-4} \times (R_{Earth}[km] + H_{orbit}[km])^{3/2} \quad (4.2)$$

$$ET[min] = P[min] \times (\phi[deg]/360) \quad (4.3)$$

- Step 3 - Check for specialized orbits

The Sun-synchronous orbit is an option of the launch providers. Its main advantage is the constant angle between the satellite and the Sun.

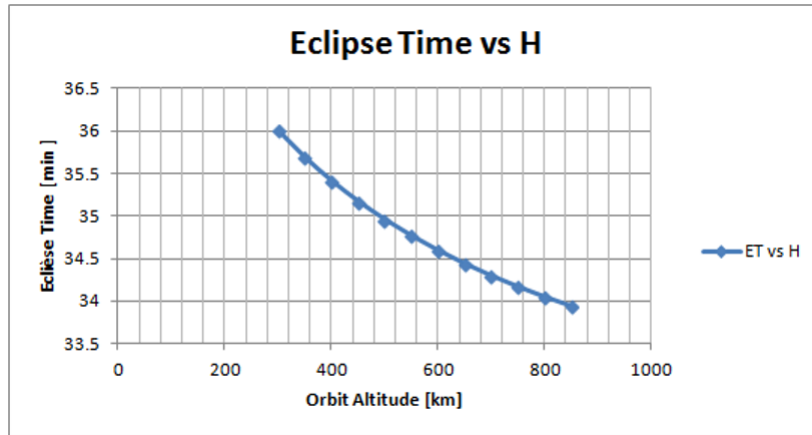


Figure 4.3: Eclipse Time [min] Vs orbit altitude [km], fixed inclination $i=11$ deg

This means that a unique value of β_S can be considered all along the mission life. A general circular LEO orbit is the alternative solution.

- Step 4 - Choose between single satellite or constellation

The cubesat platform is very well suitable for a satellites constellation. In terms of astronomical mission of detecting exoplanets the constellation arrangement would allow to observe different stars at the same time. The constellation design is not developed in this thesis work.

The other steps included in the design process are not applicable to this type of mission and to the current phase of the work (Step 5 - How orbit parameters affect the mission requirements; Step 6 - Assess launch and retrieval or disposal options; Step 7 - constellation growth and replenishment; Step 8 - create a DV budget).

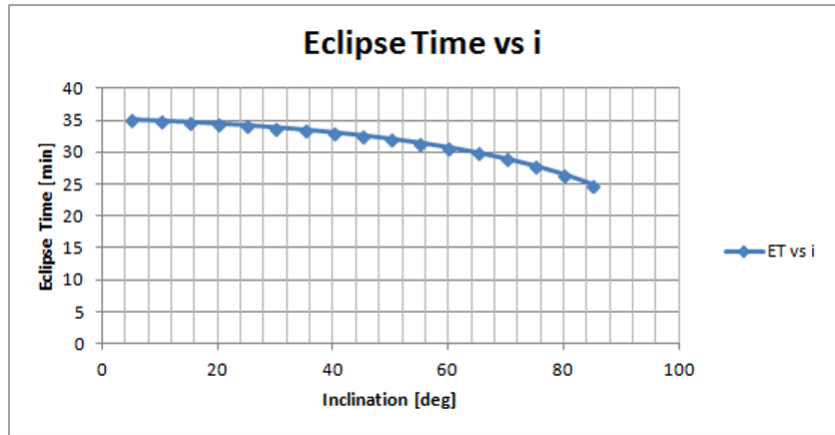


Figure 4.4: Eclipse Time [min] Vs orbit inclination [deg], fixed altitude $h=600$ km

4.6 Conclusion

The assumed orbit is circular sun-synchronous at 600 km altitude and 98° inclination, as one of the available options from the launch providers (GAUSS private company, DNEPR rocket). From this assumption the computed eclipse time is 31 minutes over 97 minutes orbital period duration. Further analysis will be conducted to identify the requirements about the straylight during the transit observation.

Chapter 5

Cubesat payload

5.1 Payload candidates description

According to the requirements, the payload should provide both photometric measurements and spectral features information. The payload selection was developed among the following options.

5.1.1 Multispectral scanning solutions

The multispectral scanning imaging techniques spatially and/or spectrally scan the scene along the time, while the spacecraft travels along its orbit. The spatial scanning consists in a line scanning of the scene and in the dispersion of one line at a time. The spectral scanning consists in the acquisition of a frame through a filter, and in changing this filter along the time. In order to fulfill the requirement of a simultaneous spectral analysis of the entire scene, both this two solutions are not selected for the current mission.

5.1.2 Multispectral not-scanning solutions

The not-scanning technique produces instead the simultaneous dispersion of the image of the entire scene or of part of it.

The first not-scanning approach is to adopt a multispectral image sensor, and the IMEC company produces two types of multispectral CMOS detectors. The Mosaic snap-shot imager (figure 5.2) consists in a CMOS detector where each macro pixel is composed by 16 (VIS) or 25 (NIR) pixels, each one sensitive to a different spectral band. With this detector each point of the scene (corresponding to each pixel of the sensor) is analyzed in a different band, and each considered band has the same sampling distance. This solution is not able to spectrally analyze each point of the scene in each considered band, and so it is not the selected solution. The Tiled IMEC imager (figure 5.1) is a CMOS detector where spectral filters are monolithically integrated on the top of the sensitive area. The detector is so divided in macro pixels, where each included pixel has the same spectral filter on the top. The available imagers provide 32 different spectral bands, that is the spectral resolution of the detector. In order to get a spectral analysis of the entire scene, this kind of detector requires the multiplication of the image, using image slicers, lenslet array or fiber-reformatting. Each copy of the image should fit the macro pixel size, in order to be entirely analyzed in one single band with a sampling distance corresponding to the number of pixels included in the macro pixel. This detector size is 2048 x 1088 pixels and considering 32 spectral bands, each macro pixel size is 256 x 272 pixels. The main drawbacks of this solution are the increased complexity of the optical design of the system, the consequent light loss and low signal for each pixel,

and the low spatial resolution of the image; also this payload option will not be selected.

A different not- scanning approach for a multispectral acquisition is to optically disperse the image, and to use a detector that is uniformly sensitive to the same spectral band.

The chosen payload configuration is this last not-scanning option, and consists in quadruplicating the image of the scene, thanks to a simple optical element, a four facets circular base pyramid. The presence of the pyramid produces also a dispersion of the image. So the final resulting image is composed of 4 copies of the star field image (partially superimposed according to the design of the prism), and the image of each object of the field is slightly spectrally dispersed. The spectral information is useful to discriminate the false event, and the image duplication ensures the redundancy in the measurement. This last option is the definitive payload choice.



Figure 5.1: IMEC tiled sensor



Figure 5.2: IMEC mosaic sensor

5.2 The payload components

The cubesat payload subsystem will be the main focus of this work. The payload consists of the following parts, Figure 5.3.

- a glass pyramid, with a round base and four facets, Figure 5.4
- a commercial objective,
- a scientific detector (cmos(1)),
- a second detector used to close the attitude control loop (cmos(2)),
- a 2-axis piezo-stage behind the detectors to compensate for the spacecraft jitter in a closed control loop.

The pyramid is located before the objective. The four pyramid facets form four images, and the four sky fields are overlapped in the sky area including the target star. The four images of the target star and surrounding sky field identify four detector areas, in which the photometric measurements take place. These are the so-called detector photometric windows, whose size can be adjusted according to the available data rate.

The pyramid allows for four simultaneous recordings of the transit, so that

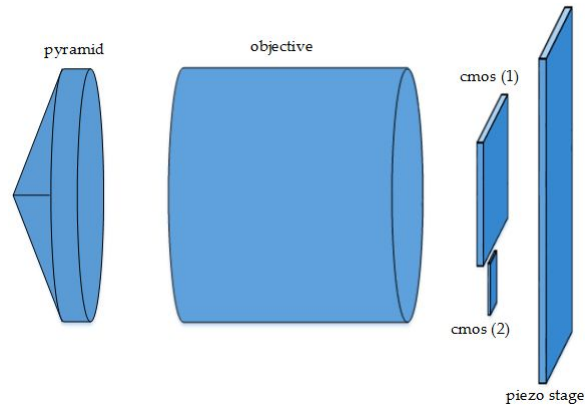


Figure 5.3: Payload Concept

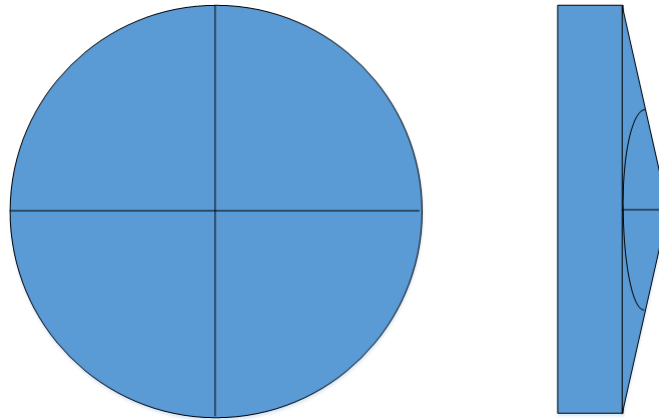


Figure 5.4: The four facets round base pyramid concept

the overall transit measurement is free from instrumental fault events due to the detector. The probability (P_4) that an instrumental fault event happens in all of the four windows is equal to the fourth power of the probability (P_1) of an instrumental fault in one window; thus P_4 is greatly lower than P_1 . The pyramid has also a dispersive power, and its spectral resolution is determined by the pyramid base angle. The dispersion direction in each photometric window is rotated of 90 degrees with respect to the neighboring

photometric windows. Before and during the transit the centroid of the photometric signal is computed in each window. If a planet transit occurs, the signal reduction is spectrally uniform and the relative distance between the windows centroids is kept constant. In case of an astronomical false positive event, the transit could be made by the star companion of a binary system, and the signal reduction is not spectrally uniform, due to the transiting star spectral emission and absorption. In this case the relative distances between the window centroids changes, Figure 5.5.

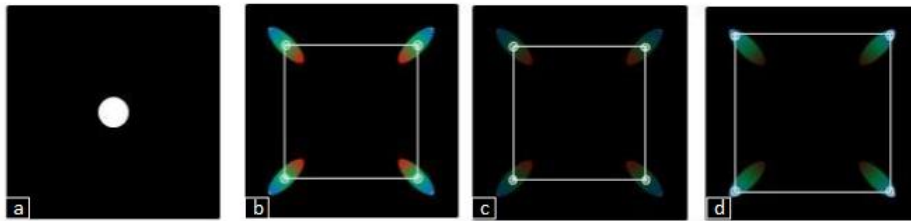


Figure 5.5: Principle of measurement. See description in the text.

In figure 5.5 the principle of measurement is depicted : (a) shows the ideal spot image of a star, as seen through the payload without the pyramid; (b) shows the ideal spot image of a star as seen through the payload with the pyramid; the four spots are dispersed and the centroids (white circles) are joined by white lines to show their relative distances; (c) shows the case of image (b) during the transit of a planet, a uniform decrement of luminosity determines no shift of centroids; (d) shows the case of image (b) during a false positive transit, the not uniform decrement of luminosity determines the shift of centroids and then the change of their relative distances.

The pyramid material first option is the commercial BK7 glass; a radiation hard glass is also considered, i.e. BK7 G18 SCHOTT, and no pyramid design variation is required. The design of the pyramid consists in the definition of the pyramid base angle according to the required rays deviation and image dispersion. To avoid saturation and to have a broad detector dynamic range, the star spot is defocused. The star defocus is assumed to be 10x10 pixels; a simplified sketch of the optical system has been realized in ZEMAX, thanks to the custom zemax library PAM2R [27], Figure 5.6. Other assumptions are: the photometric window size is 40x40 pixels, and the ray deviation from the optical axis is 300 pixels, in the two perpendicular directions on the detector plane. From geometric considerations the angular deviation α is 3.64 degrees. Considering the material reference refractive index n equal to 1.52, and according to the simplified equation 5.1 [28], the pyramid base angle δ is 7 degrees. Considering the refractive index variation in the band from 410 nm to 850 nm, each star spot is dispersed over 11 pixels, so that a bandwidth of 150 nm corresponds to 3.5 pixels. Adding in quadrature the defocus and the dispersion contribution, the total elongated star dimension is 15 pixels.

$$\delta = \alpha \cdot (n - 1) \tag{5.1}$$

The piezoelectric stage is located behind the focal plane. It is the key element to reduce the spacecraft jitter to few ppm of noise. The stage works in a closed loop that keeps the target image on the same pixels during the scientific exposure. The detector involved in the closed loop is an auxiliary sensor with a pixel size smaller than the scientific detector pixel size, and

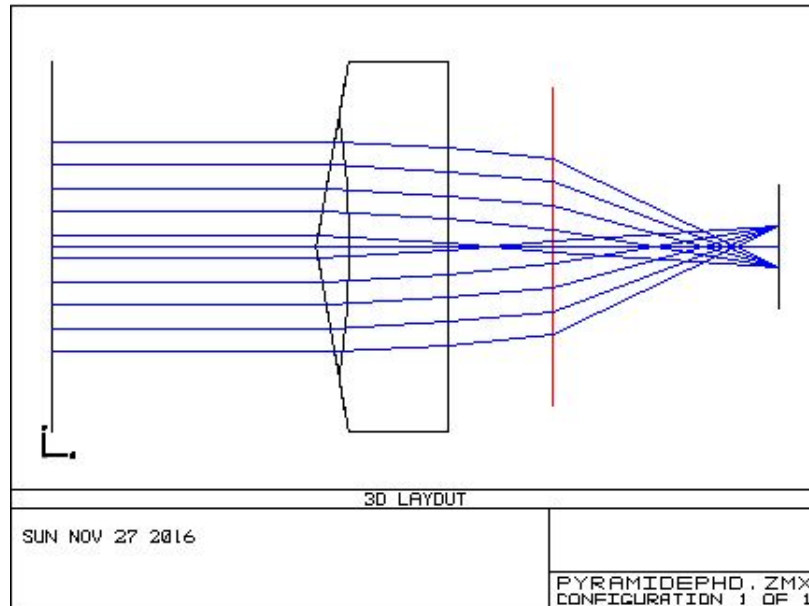


Figure 5.6: Pyramid in Zemax. The red line is the equivalent lens corresponding to the objective.

thus it reaches a higher frame rate. According to [10] this technique (together with the MIT driver code) let to reach the pointing accuracy of 2.3 arcsec.

The first stage option is a custom Physik Instrumente (PI) stage model, with custom changes to fit the cubesat platform. The two axes nanometric PI stage, PI P-733.2, has a travel range of $100 \mu\text{m}$ (for each axis) and a resolution of 0.1 nm. Another option is XY200M, a two axes piezo stage from CEDRAT Technologies, with a travel range of $200 \mu\text{m}$ (no load value) and a resolution of 20 nm.

The considered commercial objective is the ZEISS Planar T 1.4/85, with a focal length of 85 mm and the aperture diameter of 60.7 mm. The projected image on the focal plane has a diameter of 43 mm [29]. The objective has

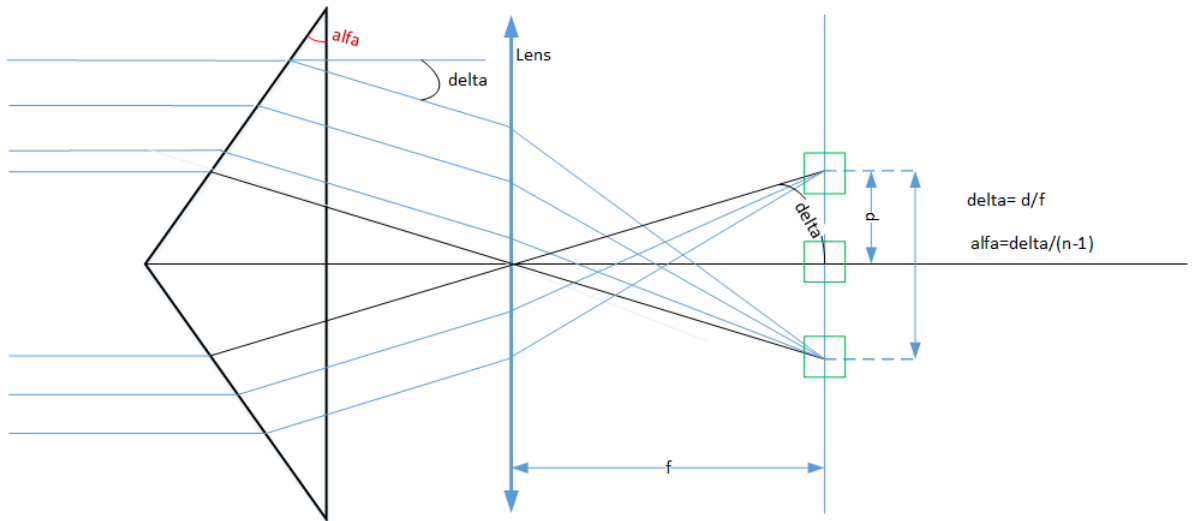


Figure 5.7: Pyramid scheme

been tested for space stresses through a scientific research work from ZEISS laboratory [30].

The selected scientific detector is the HAS2 image sensor. It is the High Accuracy Star tracker CMOS image sensor from ON Semiconductor. A second detector is used to achieve a fine attitude control (e.g. e2V EV76C454 CMOS sensor). The star tracking activity is performed from the HAS2 sensor on the image resulting from the pyramid and the objective combination, and thus the adoption of a cross-correlation algorithm is foreseen. The HAS2 features are listed in the table 5.1. The HAS temperature features are: dark current doubling for sensor temperature increment of 5.8 °C (average), and voltage-temperature variation of -4.64 mV/°C. If needed, temperature control based on a Peltier module will be considered. The HAS2 sensor has been tested for functionality up to 300 krad, and up to 42 krad the functionality is guaranteed. Additional considerations and detailed studies on this topic will

Table 5.1: HAS2 relevant characteristics

Overall dimensions	30 mm x 30 mm
Image sensor format	1024 x 1024 pixels
Pixel size	18 μm
ADC resolution	12 bit
Saturation voltage output	1.49 V
Full well capacity	$10^5 e^-$
Quantum Efficiency	45 % (500-650nm)
Spectral response	33.3 % (400-900nm)
Conversion factor	14.8 $\mu\text{V}/e$
Dark current (at 22°C)	12.5 e/pix/sec
RON	2 e/pix

be carried out in the next steps of the project. However, even at this stage, it can be noticed that this sensor is widely used in space applications such as star sensors for attitude determination whose lifetime is several years. The latter performance, even scaled down at the level of a cubesat system, will be in excess of the cubesat satellite nominal lifetime.

The payload subsystem should fit in one cubesat unit, that is in a $100 \times 100 \times 120 \text{ mm}^3$ cube, and should weight no more than 1330 g. The pyramid base height is assumed as 10 mm and the pyramid height is 3.8 mm. Table 5.3 lists the sizes and weights of each payload component; each X- and Y- size must be less than or equal to 100 mm, the sum of Z sizes must be less than or equal to 120 mm, and the sum of the weights must be less than 1330g.

Table 5.2: ZEISS objective characteristics

focal length	85 mm
F/#	1.4
Diameter	60.7 mm
Image diameter	43 mm
FOV	12.42 deg
Pixel scale	44.15 arcsec/pix

Table 5.3: List of payload components and budget of dimensions and weight for the payload unit

Component	Name	X [mm]	Y [mm]	Z [mm]	Weight [g]
Pyramid	custom, BK7 glass	62	62	13.8	85.38
Objective	Planar T* 1.4/85 ZF	77	77	62	570
Detector	HAS2	30	30	4.5	8
Detector	e2V	10	10	2	5
Imager board	custom PCB				3
Stage PI	P-733.2 CL	100	100	25	580
Stage controller	custom (on PCB)				3
Check / Tot		each \leq 100	each \leq 100	107.3	1254.38

Chapter 6

Cubesat architecture

6.1 The cubesat subsystems

Some considerations about the design of the cubesat subsystem are described in this chapter.

A summary diagram (figure 6.2, figure 6.3) is also supplied, reporting the typical functionalities, components, and size criteria. A final diagram (figure 6.4) provides an overview of the main interactions between subsystems. The payload subsystem is described in chapter 5, but it is also depicted in figure 6.4.

There is no propulsion subsystem, since no thrusters are foreseen in this cubesat.

6.2 Attitude determination and control subsystem

The system driver requirement R.1 defines that during the operative phases the payload objective must be constantly pointed toward the target star. Due to the small platform size it is far more feasible to orient the entire platform toward the target. This leads to choose a three axis control system, in zero momentum configuration.

The R.1 driver requirement defines two subsystem requirements. The first relates to a good pointing accuracy in terms of absolute angular attitude control, since the target star should be inside the field of view (FOV) and near the center of the FOV to observe a quadruplication of the image. The second most stringent subsystem requirement is the pointing stability in terms of rate of change of angular orientation.

A change of orientation could be required to expose the solar panel toward in the Sun direction. A subsystem requirement about this is still to be confirmed.

Aiming at reaching a challenging pointing stability, the chosen set of actuators is composed by: three reaction wheels, three magnetic torquers (also to desaturate the wheels), optionally control moment gyros. The chosen set of sensors is composed by: star tracker sensor, three magnetometers (in combination with the magnetotorquers), sun sensor and optionally integrated mems gyros.

Example of commercial off the shelf options are: MAI-400 from Maryland Aerospace (3 reaction wheels and 3 axis magnetometers); star tracker camera

HAS2.

Finer target pointing is achieved through a closed loop control system realized with a nanometric 2 axis stage and a second auxiliary detector (e.g. PI stage and e2V EV76C454 CMOS).

6.3 Communication Subsystem

Usually a spacecraft uplink signals consists of commands from ground station and range tones for satellite tracking. The downlink signals consists of range tones, telemetry status, and payload data. Typical commands data rate is 4000 bps, and telemetry data rate 8000 bps. Standard frequency bands for satellites are: S (2 GHz), X (8 GHz), Ku (12 GHz); for cubesat the common frequency range goes from VHF (e.g. 140 MHz) to UHF (e.g. 2.4 GHz). The assumed frequency is S band for telemetry and data.

The payload data rate per orbit can be estimated as a function of the number of frames acquired per orbit, the detector portion used for photometry, and the detector resolution. Assuming 451 frames per orbit, 4 detector portion of 40 by 40 pixel, and 12 bit resolution, the data rate per orbit is 34.6 Mbit. With a download rate of 1 Mbps (e.g. data rate of S-Band Transmitter from Nanoavionics) the time required to transmit the data to the ground station is approximately 34.6 seconds.

6.4 Command and Data Handling

The two major functions of this subsystem are : receiving, validating, decoding, and distributing commands to other spacecraft subsystems; and collecting, processing, formatting, spacecraft housekeeping and mission data for downlink or on-board use. In this cubesat mission this subsystem should manage additional tasks: the attitude algorithm to drive the 2-axis piezo stage and the storage of the detector image data. For these reason an on-board computer is foreseen.

The data storage should be compatible with the frame rate and frame size. Further future analysis will be conducted about the algorithm computation rate required by the attitude closed loop control, evaluating the possibility to use a dedicated circuit board to drive the piezo stage (as shown in figure 6.4).

The choice of the on-board computer will be done among commercial off the shelf single board computer suitable for cubesats.

The computer interfaces must be compatible with the output connectors of the detectors and (if used) of the piezo stage.

6.5 Thermal control subsystem

The role of this subsystem is to keep all the components within the range of their required temperature limits in each mission phase. This means to keep the components within the operating temperature limits during the mission active phases, and within the survival temperature limits in the rest of the

mission. Also thermal gradient requirements, that could induce structural deformations, are fulfilled through this subsystem.

The sources of heat are solar radiation, Earth-reflection and infrared radiation, and electrical energy dissipated in electrical components. Usually electronics can stand a temperature range of $20\text{ }^{\circ}\text{C} \pm 20\text{ }^{\circ}\text{C}$, while battery cells are more sensitive to temperature, and perform best in the range of $5\text{--}20\text{ }^{\circ}\text{C}$.

Due to the limited available space of this cubesat platform, a passive thermal control is chosen, and a more detailed analysis will be conducted in next phases of the project.

6.6 Electrical Power Subsystem

Electrical power is provided by solar panel. Table 6.1 describes a first estimated power budget. The budget specifies the power required in the eclipse phase (P_e), in the daylight phase while communicating with the ground station (P_{d1} , *Daylight1* phase), and in the daylight phase without communication with ground station (P_{d2} , *Daylight2* phase). The total orbit duration is 97 minutes, the eclipse phase duration is 31 minutes, (T_e), the *Daylight1* phase duration is assumed equal to 20 minutes (T_{d1}), and the *Daylight2* phase duration is assumed equal to 46 minutes (T_{d2}).

The required solar panel area is computed in the following steps.

- The power control technique should consist in a peak-power tracker subsystem, so the efficiency of the path from the solar array to the

load through the batteries, X_e , is assumed as 0.6, and the efficiency of the path from the solar array to the load directly, X_d , is assumed as 0.8.

- The power that the solar array must provide during daylight to power the spacecraft in the entire orbit is P_{sa} , according to equation 6.1.
- The selected solar cell is a silicon cell with efficiency of 14.8 %, so that the ideal solar cell output performance, P_o , is 202.32 W/m².
- The inherent degradation due to the solar cell assembly, I_d , is assumed as 0.77 as nominal value. The Sun incidence angle is considered as in the worst case, thus equal to 23.5 deg. Then the power output at the beginning of life, P_{BOL} , is 142.86 W/m².
- Solar array typical degradation in LEO orbit is 3.75 % per year, and considering a life time of 4 years the power output at the end of life, P_{EOL} , is 122.61 W/m².
- Finally the required solar array area, A_{sa} , is the ratio between the required power to be acquired by the solar array, P_{sa} , and the its output power at the end of life, P_{EOL} . The estimated value is 117 562.91 mm².

One cubesat major face extension is 100 mm x 300 mm. A panel array of 5 panels, each one of area equal to one cubesat major face, would provide a total area of 150 000 mm². During the launch the five panels are kept wrapped around the cubesat structure, and then in orbit the array is

deployed in a configuration like one suggested in figure 6.1.

The energy storage is provided by secondary batteries. The choice of the battery requires an estimation of its watt-hour capacity. The assumed mission lifetime is 4 years. As mentioned before, the orbital period is 97 minutes and the orbital eclipse time is 31 minutes, so the number of eclipses per day is 14.85, and the number of eclipses per lifetime is 21 674.23. The power required during the eclipse phase is P_e . The considered value for the Depth Of Discharge, DoD , is 0.2, since typical value for LEO orbits are in the range of 15-25%. The transmission efficiency between the battery and the load, n , is 0.90, and for this calculation the number of batteries, N , is kept equal to one. The required battery capacity, C_r , is 18.20 Whr, as reported in table 6.2. For instance commercial off-the shelf options available for cubesats are: GOMSpace Lithium ion battery (model: BP4, up to 38.5 Whr), ClydeSpace lithium polymer cells battery (model: CS 1U Power Bundle, including Electrical Power Subsystem and 20Whr battery), Endurosat lithium polymer cells battery (model: Power module PLUS, including Electrical Power Subsystem and 20 Whr battery).

$$P_{sa} = \frac{\frac{P_e \cdot T_e}{X_e} + \frac{P_{d1} \cdot T_{d1}}{X_d} + \frac{P_{d2} \cdot T_{d2}}{X_d}}{T_{d1} + T_{d2}} \quad (6.1)$$

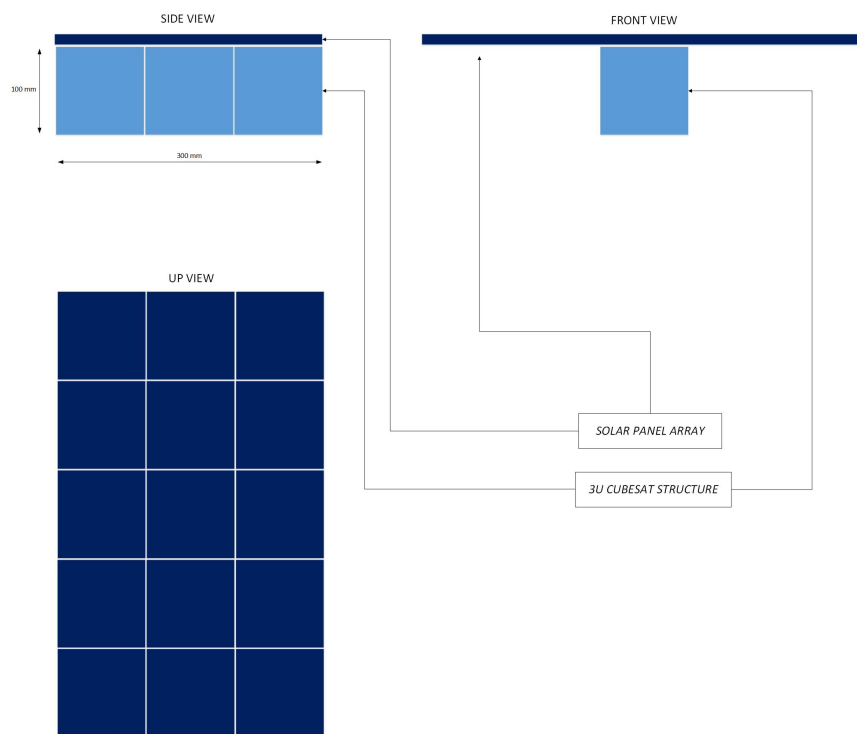


Figure 6.1: Scheme of solar panel array configuration

Table 6.1: Power budget

Component Type	Name	P on [mW]	P_e	P_{d1}	P_{d2}	I max [mA]	V [V]
Payload Detector/star tracker	HAS2	110.55	on	on	on	33.5	3.3
Payload secondary Detector imager board	e2V custom PCB (hp)	80 100	on on	off on	off on		3.3 - 1.8
Payload/ ADC Stage	PI P-733.2 CL (hp)	100	on	off	off		
Payload/ ADC stage controller	custom (on PCB) (hp)	100	on	off	off		
Antenna nanoavionics	S-Band Transceiver	4950	off	on	off	1500	3.3
On board computer GOM space include 3 magnetotorquers and 3 mems gyros	NanoMind A3200	3300	on	on	on	1000	3.3
Reaction wheels hyperion	RW210	2550	on	on	on		3.3
TOT		11290.55	6340.55	11010.55	6060.55		

6.7 Structure Subsystem

The structure size relates to one of the mission system drivers, i.e. to achieve the mission objective through a 3 (or 3+) units platform for cubesat. The structure frame material is aluminium and it is chosen among the commercial off-the-shelf options, such as ClydeSpace 3U solution.

Table 6.2: Solar array required area and battery sizing

T_{d1}	20	min
T_{d2}	46	min
T_e	31	min
P_{d1}	11010.55	mW
P_{d2}	6060.55	mW
P_e	6340.55	mW
X_e	0.6	
X_d	0.8	
P_{sa}	14.41	W
η	14.8 %	
P_o	202.32	W/m ²
I_d	0.77	
θ	23.5	deg
P_{BOL}	142.86	W/m ²
degrad/year	3.75 %	
P_{EOL}	122.61	W/m ²
A_{sa}	117 562.91	mm ²
Design Area	150 000	mm ²
Life Time	4	years
eclipse/day	14.85	
DOD	0.2	
n	0.9	
N	1	
C_r	11.19	Whr

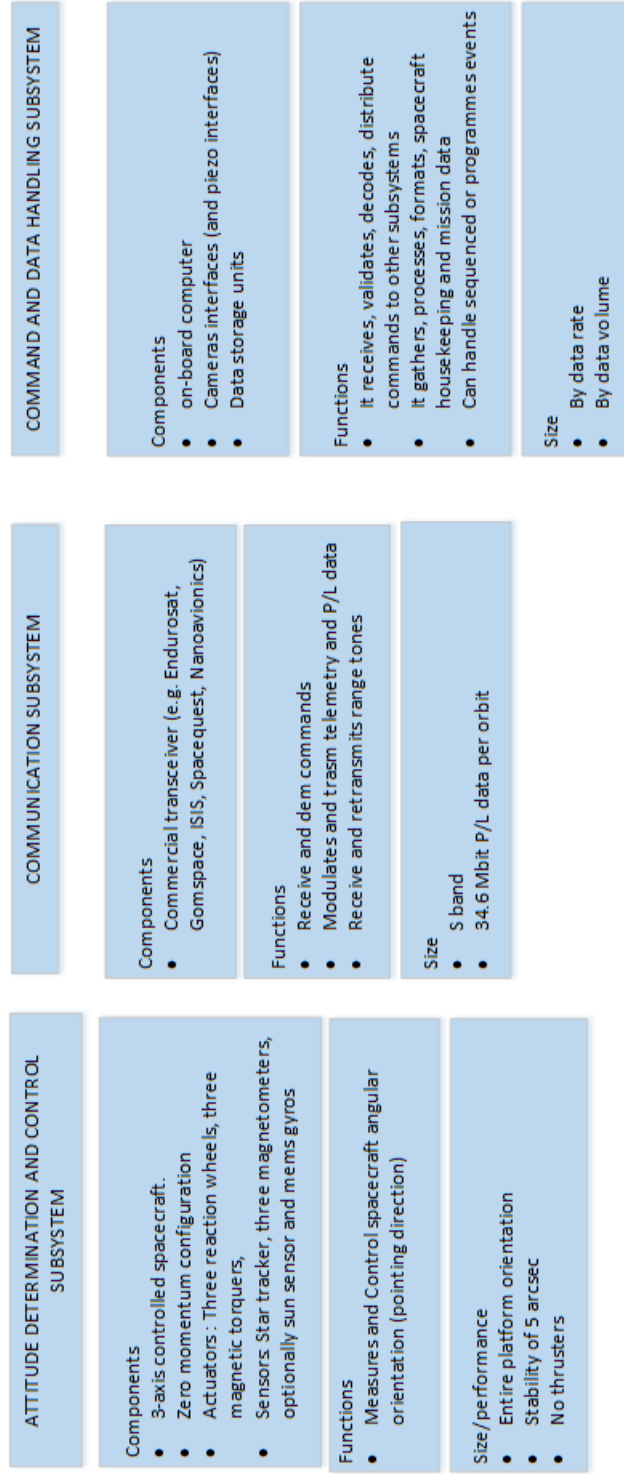


Figure 6.2: Scheme of subsystems configuration -1

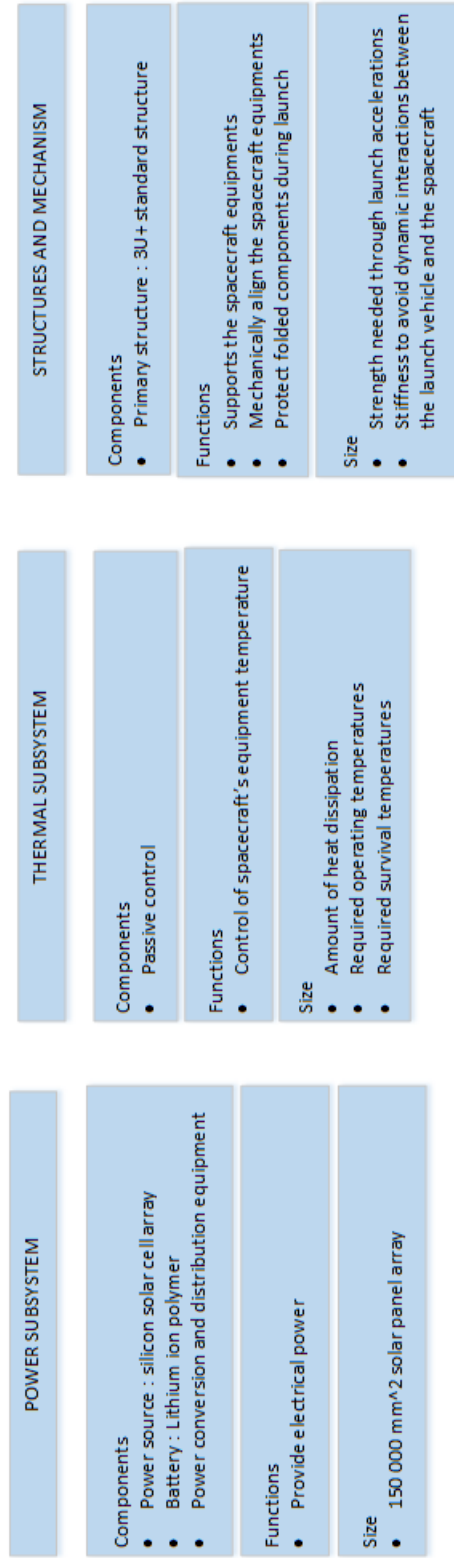


Figure 6.3: Scheme of subsystems configuration -2

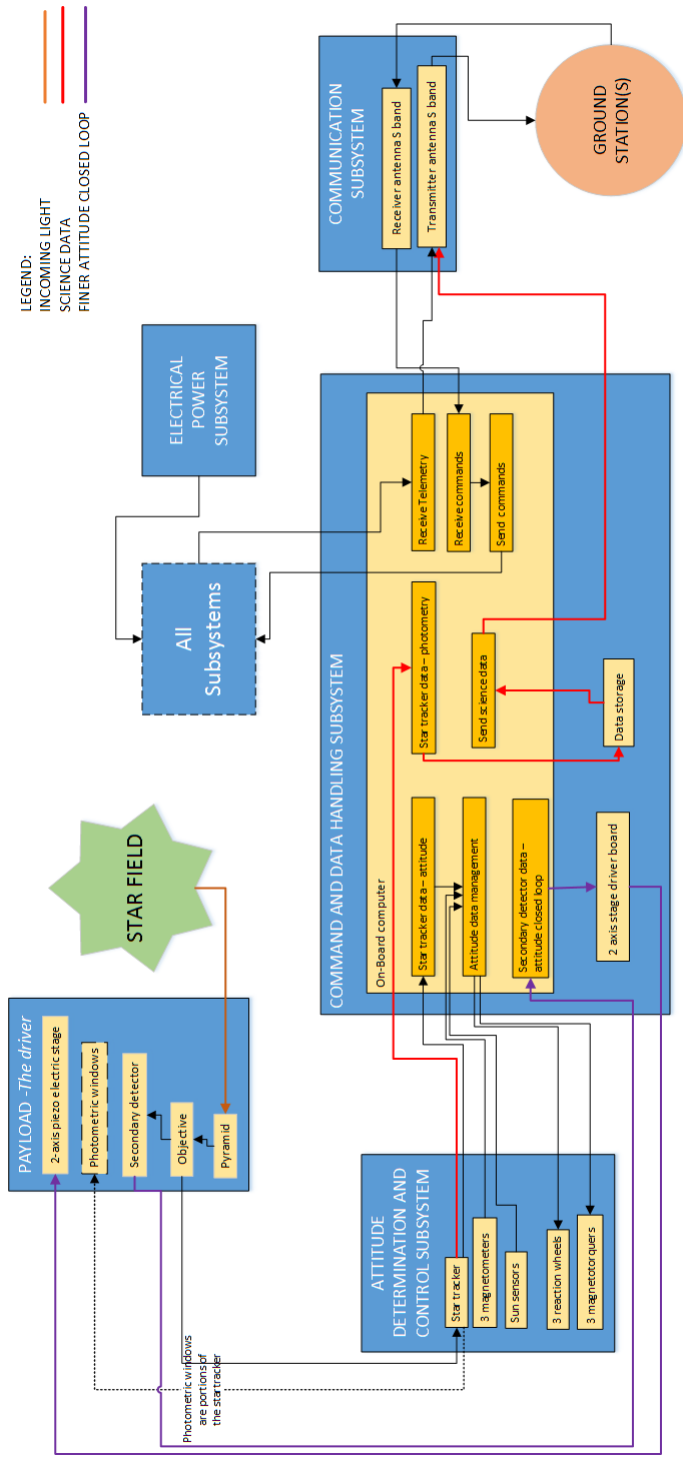


Figure 6.4: Scheme of subsystems interaction

Chapter 7

Mission Target

7.1 Star visual magnitude limit

The most demanding requirement refers to the capability of detecting the signal with amplitude equal to 84 ppm and with maximum noise level of 12 ppm. There is a limit in the target star V-magnitude, below which this requirement is fulfilled. This limit is computed following the steps.

The output detector image includes four measurements of the planet transit across the target star. This image can be postprocessed (P) in two ways.

To enhance the detected signal level, the absolute value of the transit measurement is derived by adding together the four measurements of each photometric window. The false positive check can be performed by the relative comparison of the centroid location in each photometric window.

A second option is to measure the absolute value of the transit decrement in each of the four photometric windows, getting then four absolute measurements of the transit. Similarly to the previous case, the false positive check

can be performed by the relative comparison of the centroid location in each photometric window.

The constraints related to the achievable S/N are the followings, table 7.1.

- The observation time on each orbit (i.e. the product between the exposure time of a single frame and the number of co-added frames) must be less than or equal to the duty cycle time. The total transit observations should include one full transit time before and after the transit, to better estimate the transit baseline.
- The exposure time of each frame must be less than the time required to saturate the detector. This constrain is expressed as the number of photons corresponding to the saturation voltage, taking into account the detector conversion factor and the quantum efficiency.

For both ways of postprocessing the computational steps to identify the star visual magnitude limit are the same, but with different starting data. The steps are described in the following.

1. Evaluation of the incoming photon flux from typical target stars. The considered V-magnitude (vmag) range is from 0 to 5. The photon flux s_{flux} is given in photons per seconds, scaling the reference photon flux of Vega in the visible band. The assumed optical aperture is the one from Zeiss objective ($2893 (mm)^2$).

The overall signal level is then computed in terms of detected photons, considering a range of possible exposure time t_{exp} from 0.01 s to 10 s, and of a number of co-added frames ($\#Frames$) from 1 to 10000, equation 7.1.

2. Noise computation. The noise sources taken into account are: photonic noise (N_{phot}), dark current noise (N_{dark}), and read out noise (N_{ron}) [31], equation 7.2 7.3 7.4. The detector choice sets the dark current value (I_{dark}), expressed in electrons per pixel per seconds, and the read out characteristic (RON), expressed in electrons per pixel, and the two relative noise sources are functions of the number of read pixels.
3. Signal to noise ratio computation, equation 7.5. The dominant noise source is the photon noise, and the S/N can be approximated as the square root of the signal, equation 7.6. The requirement of maximum noise level of 12 ppm corresponds to a S/N of 10^5 , and requires a star signal level of 10^{10} photons. The star spot is intentionally defocused to improve the dynamic range, and the star photons are spread on 10×10 pixels, leading to 10^8 photons per pixel required. A detector resolution of 12 bit provide 4096 quantization levels. Considering each pixel receiving 10^8 photons, each level differs of $2.44 \cdot 10^4$, that is lower than the transit signal value (i.e. 10^5).
4. Computation of the minimum number of frames to be added together

to reach the required signal to noise per pixel, and to remain below the saturation limit of the detector. According to the detector choice, the saturation limit is $2.237 \cdot 10^5$ [phot/pix], and the minimum number of frames to reach 10^8 photons per pixel is 447.

5. Computation of the maximum exposure time per frame. According to the orbit choice, the duty cycle time to observe the planet transit is 31 min (1860 s). The ratio between the duty cycle time and the minimum number of co-added frames (447) determines the maximum integration time per frame, 4 s.
6. For each star magnitude in the considered magnitude range, computation of the maximum exposure time, t_{lim} , to get the highest detector voltage with one frame. The star flux is spread on 10x10 pix.
7. Computation of the number of co-added frames, $\#Frames_{s/n}$, required to get a S/N of 10^5 (star signal of 10^{10}).

$$s = s_{flux} \cdot \eta_{sys} \cdot t_{exp} \cdot \#Frames \quad (7.1)$$

$$N_{phot}^2 = s \quad (7.2)$$

Table 7.1: Limiting v-magnitude computation entries

Constraints	
Duty cycle time	31 min (1860 s)
Photons to saturate:	$2.237 \cdot 10^5$ [phot/pix]
Requirements	
S/N	$\geq 10^5$
Photons per pixel:	10^8
Assumptions	
window:	40x40 pix
system efficiency:	70%
Star defocus:	10x10 pix

$$N_{dark}^2 = I_{dark} \cdot \#pix \cdot t_{exp} \cdot \#Frames \quad (7.3)$$

$$N_{RON}^2 = \#pix \cdot RON \cdot \#Frames \quad (7.4)$$

$$\frac{S}{N} = \frac{s}{\sqrt{N_{phot}^2 + N_{dark}^2 + N_{RON}^2}} \quad (7.5)$$

$$\frac{S}{N} \approx \sqrt{s}^1 \quad (7.6)$$

¹If readout noise and dark noise are negligible

Table 7.2: Results- First postprocessing option

vmag=0,	tlim=0.17 s	frames=451 ;
vmag=1,	tlim=0.43 s	frames=451 ;
vmag=2,	tlim=1.09 s	frames=451 ;
vmag=3,	tlim=2.74 s	frames=451 ;
vmag=4,	tlim=6.89 s	frames=453 ;
vmag=5,	tlim < 10 s	frames=461 ;

7.1.1 First postprocessing option

In the first postprocessing option the considered incoming flux is the star photon flux s_{flux} , and the considered read pixel are the four photometric windows of 40x40 pixels each.

The results of the computation show that star V-magnitude equal to 3 is the limit, since the observation of a star of fourth V-magnitude would require an exposure time longer than 4 seconds. A finer analysis in the magnitude range from 3 to 4 shows that the limiting V-magnitude is 3.38 (Figure 7.1, Table 7.2).

7.1.2 Second postprocessing option

In the second postprocessing option the considered incoming flux is star photon flux s_{flux} divided by four, and the considered read pixel are these of one photometric window of 40x40 pixels each.

The results of the computation show that star V-magnitude equal to 1.78 is the limit. (Figure 7.2, Table 7.3).

Table 7.3: Results- Second postprocessing option

vmag= 0	tlim= 0.68	frames=464.03
vmag= 0.20	tlim= 0.81	frames=464.03
vmag= 0.40	tlim= 0.98	frames=464.03
vmag= 0.60	tlim= 1.18	frames=464.03
vmag= 0.80	tlim= 1.43	frames=451.51
vmag= 1.00	tlim= 1.73	frames=451.51
vmag= 1.20	tlim= 2.08	frames=451.51
vmag= 1.40	tlim= 2.51	frames=451.51
vmag= 1.60	tlim= 3.01	frames=451.51
vmag= 1.80	tlim= 3.61	frames=451.51
vmag= 2.00	tlim= 4.36	frames=451.51
vmag= 2.20	tlim= 5.23	frames=451.51
vmag= 2.40	tlim= 6.28	frames=451.51
vmag= 2.60	tlim= 7.56	frames=464.03
vmag= 2.80	tlim= 9.11	frames=451.51
vmag= 3.00	tlim= 10.96	frames=464.03
vmag= 3.20	tlim= 13.16	frames=464.03
vmag= 3.40	tlim= 15.84	frames=464.03
vmag= 3.60	tlim= 19.04	frames=464.03
vmag= 3.80	tlim= 20.00	frames=526.60
vmag= 4.00	tlim= 20.00	frames=639.23

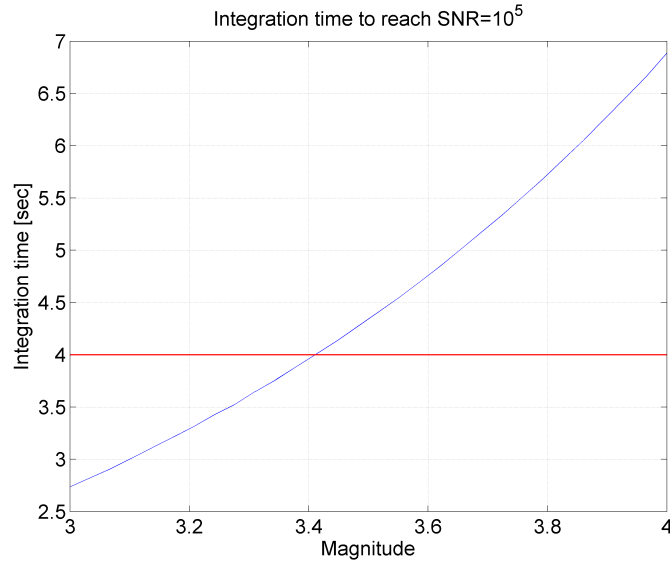


Figure 7.1: First postprocessing option. Integration time as function of target star V-magnitude. The SNR is 10^5 . The red line is the maximum integration time limit, i.e. 4 seconds.

7.2 Target Star

It is more affordable to detect transit around dwarf stars than around giant stars. This because the signal decrement is proportional to the square ratio between the planet radius and the star radius, and in the latter case the stellar diameter is so large that the signal decrement is almost undetectable. For this reason the target selection is limited to dwarf stars.

The number of known dwarf stars (luminosity class V) of V-magnitude less than four is 115 (91 dwarfs have V-magnitude less than 3.8)². Currently (February 2017) there are 4 confirmed exoplanets orbiting around dwarf stars of V-magnitude less than 4, and 6 unconfirmed exoplanets orbiting around

²From SIMBAD astronomical database, <http://simbad.u-strasbg.fr/simbad/>

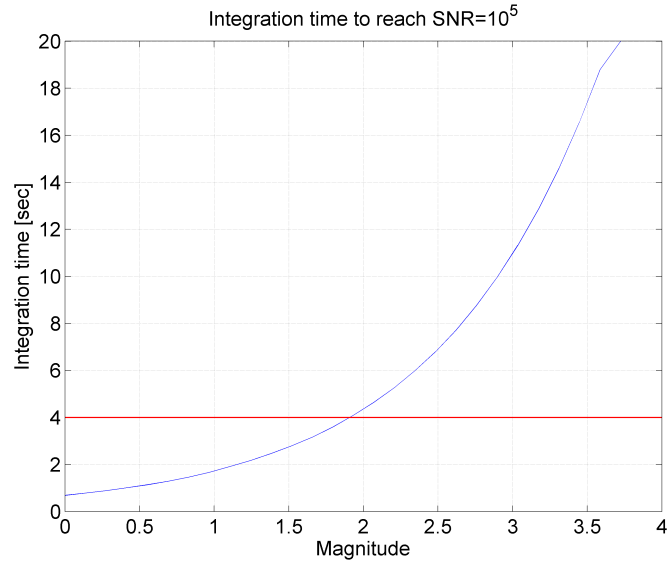


Figure 7.2: Second postprocessing option. Integration time as function of target star V-magnitude. The SNR is 10^5 . The red line is the maximum integration time limit, i.e. 4 seconds.

the same type of star, table 7.4 ³ and figure 7.3 7.4 7.5 7.6. None of them has been ever observed with the photometric method from space. One of the confirmed exoplanet host star is Alpha Centauri B (planet Alpha Centauri Bb), and further investigations are required for the star companion Alpha Centauri A. First option target is Alpha Centauri AB, that is the closest-to-the-Sun binary star system that could host a planet in the habitable zone, and it is the most feasible target to be observed from a small platform [32]. Alpha Centauri A V-magnitude is 0.01, and Alpha Centauri B V-magnitude is 1.33. It is still to be defined the observing strategy, e.g. switching from one star to the companion, or choosing one of the two as permanent target.

³From <http://exoplanet.eu/>

Table 7.4: Exoplanets

Star name	planet letter	detection type	vmag	type	status
Fomalhaut	b	Imaging	1.16	A3V	Confirmed
alpha Cen B	b	Radial Velocity	1.33	K1V	Confirmed
beta Pic	b	Imaging	3.86	A6V	Confirmed
eps Eridani	b	Radial Velocity	3.73	K2 V	Confirmed
eps Eridani	c	Other	3.73	K2 V	Unconfirmed
tau Cet	b	Other	3.5	G8.5V	Unconfirmed
tau Cet	c	Other	3.5	G8.5V	Unconfirmed
tau Cet	d	Other	3.5	G8.5V	Unconfirmed
tau Cet	e	Other	3.5	G8.5V	Unconfirmed
tau Cet	f	Other	3.5	G8.5V	Unconfirmed

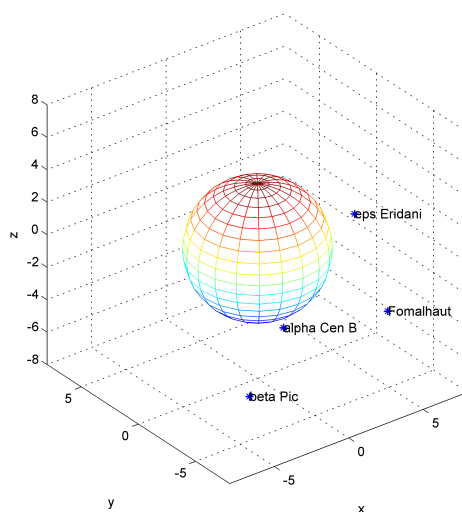


Figure 7.3: Location of exoplanets hosting star of V class and $vmag \leq 4$ on the 3D celestial sphere.

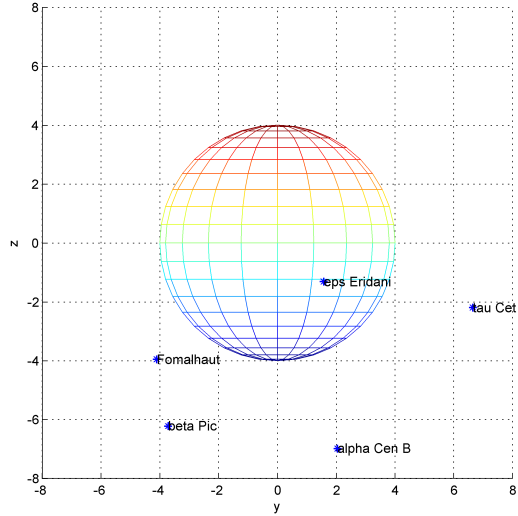


Figure 7.4: Location of exoplanets hosting star of V class and $v_{\text{mag}} \leq 4$ on the 2D celestial plane.

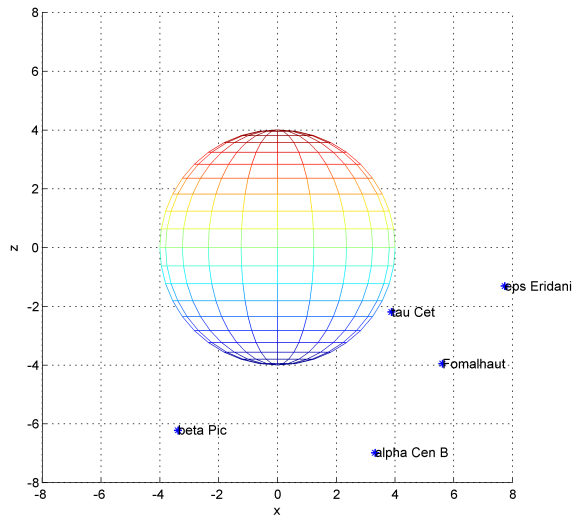


Figure 7.5: Location of exoplanets hosting star of V class and $v_{\text{mag}} \leq 4$ on the 2D celestial plane

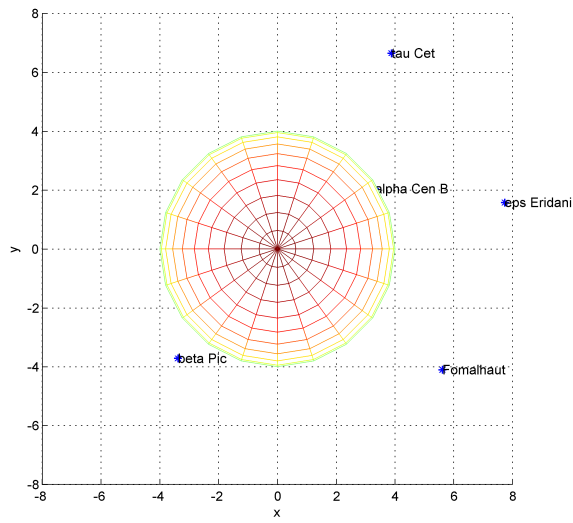


Figure 7.6: Location of exoplanets hosting star of V class and $v_{\text{mag}} \leq 4$ on the 2D celestial plane

Chapter 8

Payload functional simulation

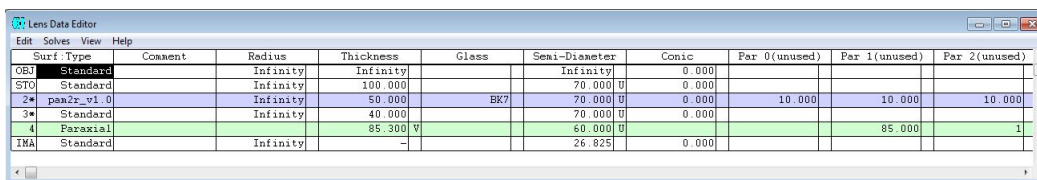
A first payload design check has been developed through the theoretical output images and analysis provided by the software Zemax.

The object is set to infinity. The aperture stop is set on the first surface. The considered aperture diameter is 80 mm. The pyramid is modeled thanks to the custom zemax library PAM2R. This library allows to define the four pyramid base angles, the diameter aperture, the base thickness, and the material, that is assumed to be standard BK7.

The next surface defines the distance between the pyramid and the ZEISS objective. The objective is here included as an equivalent lens, paraxial surface, at a distance of 40 mm from the pyramid, with focal length equal to 85 mm, and aperture of 60 mm. The last surface define the image plane, and it is located at a distance of 85.3 mm, so that the introduced defocus of 300 micron provides a dispersed spot of a dimension comparable to 10 pixels, figure 8.1, figure 8.3, figure 8.4.

Figure 8.2 shows the ray tracing for off axis fields of 12 degrees and -12 degrees.

Figure 8.5 shows an example image coming from the on axis field, developed by geometrical ray tracing and propagated till the detector surface, which is assumed to be composed by 1000 x 1000 pixels. The number of propagated rays is 10^6 . The lateral grayscale bar is proportional to the detector pixel value.



Surf	Type	Comment	Radius	Thickness	Glass	Semi-Diameter	Conic	Par 0 (unused)	Par 1 (unused)	Par 2 (unused)
OBJ	Standard		Infinity	Infinity		Infinity	0.000			
STO	Standard		Infinity	100.000		70.000 U	0.000			
2*	panzr_v1.0		Infinity	50.000	BK7	70.000 U	0.000	10.000	10.000	10.000
3*	Standard		Infinity	40.000		70.000 U	0.000			
4	Paraxial		85.300 V			60.000 U			85.000	1
IMA	Standard		Infinity	-		26.825	0.000			

Figure 8.1: Optical configuration

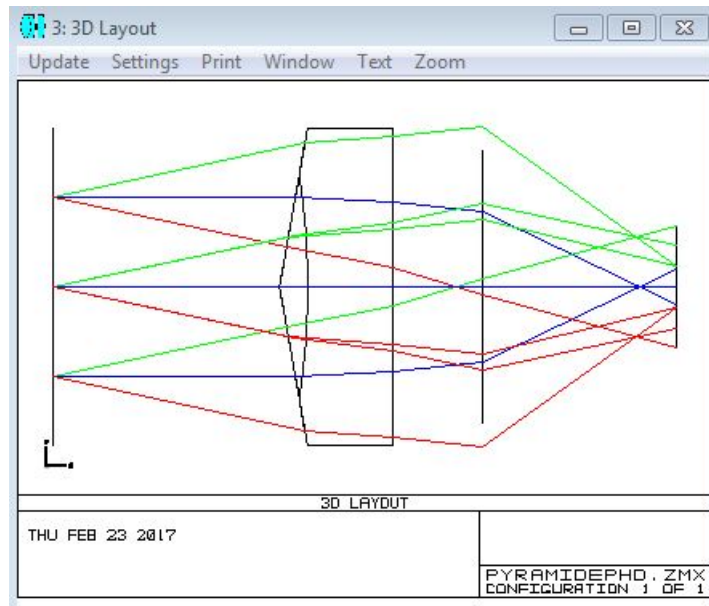


Figure 8.2: Optical configuration - on axis field, 12 deg field, and -12 deg field

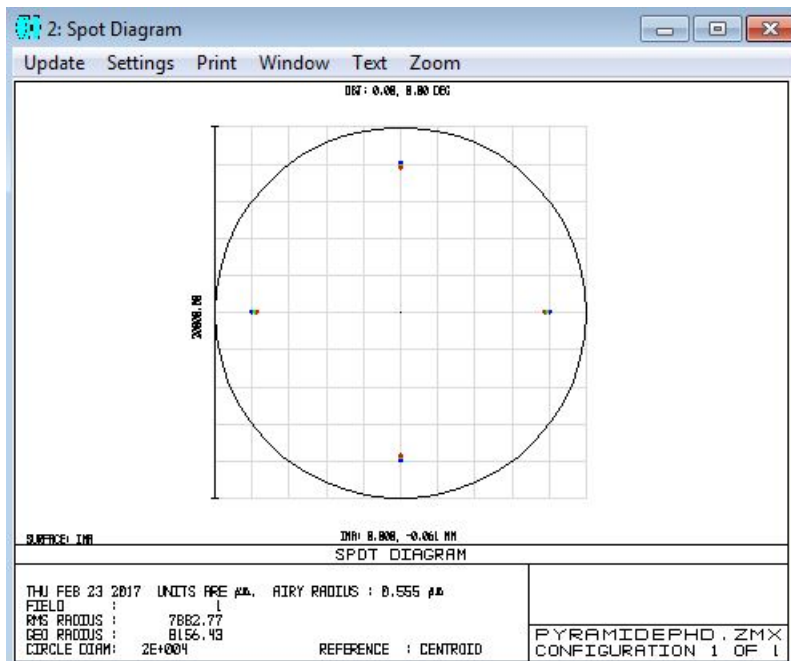


Figure 8.3: Spot diagram

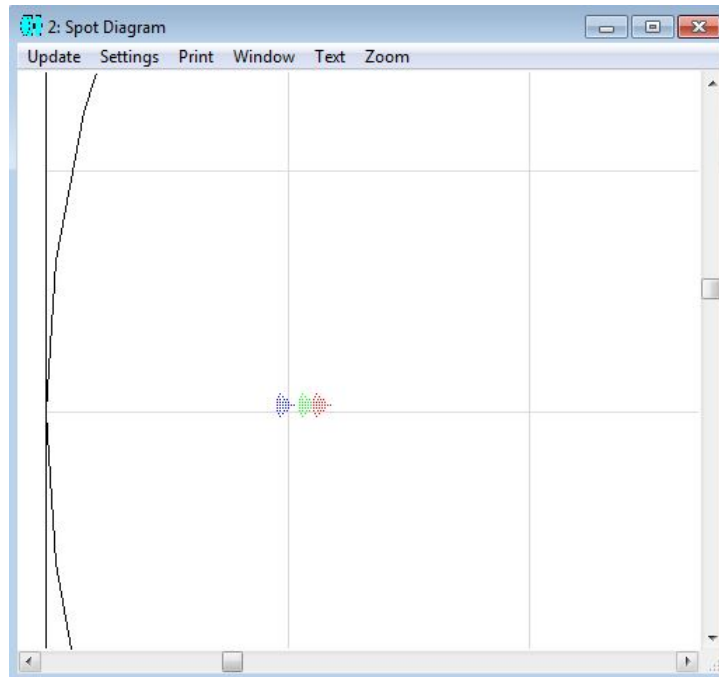


Figure 8.4: Spot diagram - zoomed view

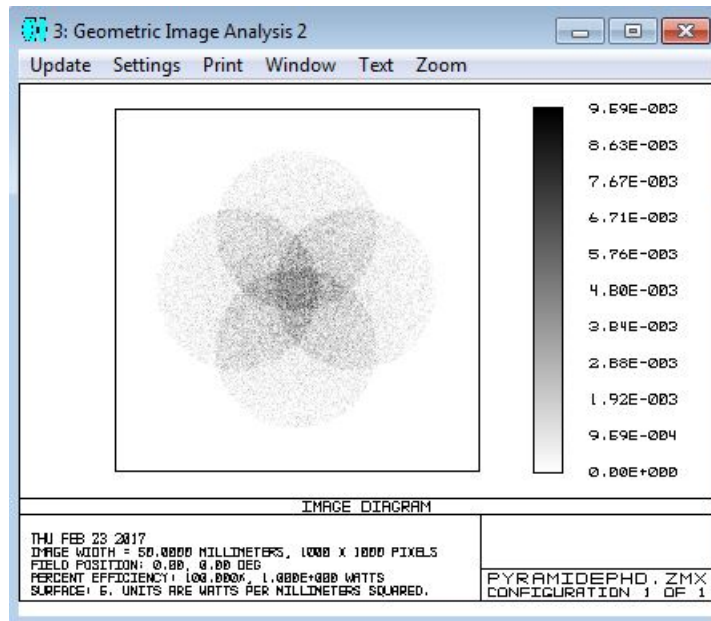


Figure 8.5: Geometric image analysis- on axis field

Chapter 9

Conclusion

This work is intended to be a starting point of a feasibility analysis to develop an astronomical mission of this type from a cubesat platform. The aim of this thesis is also to provide a quite complete overview of the major aspects concerning the mission, with a deeper focus on the payload subsystem. The possibility to provide a turnkey and cheap platform to achieve astronomical objective related to exoplanets raises interest among astronomers for scientific reason, and also among engineers for the attractive technical challenge.

9.1 Contributions

The academic supervisors Prof. Accardo and Prof. Rufino are stimulating tutors, that guided the research from the engineering point of view. The optical layout idea has been developed in collaboration with Dr. Ernesto Oliva, a senior researcher from the astrophysical observatory of Arcetri (national astrophysical research institute - INAF), and with Dr. Andrea Tozzi, a se-

nior researcher from the same institute. The great news of the development of the custom zemax library PAM2R has been provided to me by Dr. Pietro Schipani, who also provided extensive support in training and question session about the program and the library, together with Dr. Demetrio Magrin.

9.2 Future Work

The foreseen activities are the followings.

- to complete the simulation regarding the pointing stability, assuming a tilt amount, a quantum efficiency inter pixel variation on the detector, and evaluating the consequences on the measurement performance;
- to simulate a scientific measurement on the chosen target;
- to develop a hardware demonstrator of the finer attitude closed control loop.

Bibliography

- [1] Sara Seager, editor. *Exoplanets*. University of Arizona Press, Tucson : Houston, January 2011.
- [2] E. Bernieri. Laboratorio di astrofisica. Technical report, Univeristy Of Roma tre, 2011.
- [3] Francesco Martino. *Stelle e sistemi stellari*. Italo Bovolenta Editore, 1987.
- [4] S. Aigrain, P. Barge, and et al. The corot exoplanet programme: Exploring the gas-giant/terrestrial planet transition. *Proceedings of 14th Cambridge Workshop on Cool Stars, Stellar Systems, and the Sun*, 384(1):270, 2007.
- [5] M. Auvergne, P. Bodin, and et al. Boissard, L. The CoRoT satellite in flight: description and performance. *A&A*, 506(1):411–424, October 2009.
- [6] William Borucki, David Koch, and et al. Batalha, Natalie. KEPLER: Search for Earth-Size Planets in the Habitable Zone. *Proceedings of the International Astronomical Union*, 4(S253):289–299, 2008.
- [7] George R. Ricker, Joshua N. Winn, and et al. Vanderspek, Roland. Transiting Exoplanet Survey Satellite. *Journal of Astronomical Telescopes, Instruments, and Systems*, 1(1):014003–014003, 2014.
- [8] Andrea Fortier, Thomas Beck, Willy Benz, Christopher Broeg, Virginie Cessa, David Ehrenreich, and Nicolas Thomas. CHEOPS: a space telescope for ultra-high precision photometry of exoplanet transits. volume 9143, pages 91432J–91432J–12, 2014.

- [9] H. Rauer, C. Catala, C. Aerts, T. Appourchaux, and et al. The PLATO 2.0 mission. *Experimental Astronomy*, 38(1):249–330, 2014.
- [10] Matthew Smith, Sara Seager, Christopher Pong, Matthew Knutson, and David Miller. The exoplanetsat mission to detect transiting exoplanets with a cubesat space telescope. In *Proc. 25th annual AIAA/USU Conference on Small Satellites*, 2011.
- [11] Eberhard Grun, Bo A. S. Gustafson, Stan Dermott, Hugo Fechtig, I. Appenzeller, G. Gorner, M. Harwit, R. Kippenhahn, J. Lequeux, P. A. Strittmatter, and V. Trimble, editors. *Interplanetary Dust*. Astronomy and Astrophysics Library. Springer Berlin Heidelberg, Berlin, Heidelberg, 2001.
- [12] Jae-Pil Park, Sang-young Park, and et al. Lee, Kwangwon. Mission Analysis and CubeSat Design for CANYVAL-X mission. In *SpaceOps 2016 Conference*, SpaceOps Conferences. American Institute of Aeronautics and Astronautics, May 2016.
- [13] K. Cahoy, A. Maritan, and et al. Cubesat deformable mirror demonstration. In *Proceedings of the Space Telescopes and Instrumentation 2012: Optical, Infrared, and Millimeter Wave*, 2012.
- [14] M. Nowak, S. Lacour, V. Lapeyre, L. David, A. Crouzier, C. Dufoing, H. Faiz, T. Lemoult, and P. Tr  buchet. Reaching sub-millimag photometric precision on Beta Pictoris with a nanosat: the PicSat mission. volume 9904, pages 99044L–99044L–7, 2016.
- [15] Jon M. Jenkins. The impact of solar-like variability on the detectability of transiting terrestrial planets. *The Astrophysical Journal*, 575(1), 2002.
- [16] A. Santerne, F. Fressin, R. F. D  az, P. Figueira, J.-M. Almenara, and N. C. Santos. The contribution of secondary eclipses as astrophysical false positives to exoplanet transit surveys. *A&A*, 557, September 2013.
- [17] Jeffrey L. Coughlin and Susan E. Thompson and Stephen T. Bryson, et al. Contamination in the Kepler Field. Identification of 685 KOIs as False Positives via Ephemeris Matching Based on Q1-Q12 Data. *The Astronomical Journal*, 147(5):119, 2014.

- [18] A. Santerne, C. Moutou, F. Tsantaki, M. and Bouchy, G. HÃ©brard, V. Adibekyan, J.M. Almenara, L. Amard, S.C. Barros, and I Boisse. Sophie velocimetry of kepler transit candidates. *Astronomy and Astrophysics*, 587(A64), 2016.
- [19] J. Almenara, M., H. Deeg, J., and et al. Aigrain, S. Rate and nature of false positives in the CoRoT exoplanet search. *A&A*, 506(1):337–341, October 2009.
- [20] Stephen T. Bryson and Jon M. Jenkins and Ronald L. Gilliland, et al. Identification of Background False Positives from Kepler Data. *Publications of the Astronomical Society of the Pacific*, 125(930):889, 2013.
- [21] Wiley J. Larson and James R. Wertz. *Space Mission Analysis and Design*, chapter 1-4, 9. Microcosm Press and Kluwer Academic Publishers, 1999.
- [22] Jon M. Jenkins and Douglas A. Caldwell and William J. Borucki. Some Tests to Establish Confidence in Planets Discovered by Transit Photometry. *The Astrophysical Journal*, 564(1):495, 2002.
- [23] Riki Munakata. Cubesat design specification. Technical report, California Politechnic State University, 2009.
- [24] Anne Ytterskog and Anna Rathsman. Rainbow- a launch capability for small satellites from esrange, sweden. In *Proc. 29th annual AIAA/USU Conference on Small Satellites*, 2015.
- [25] GAUSS srl Group of Astrodynamics for the use of space systems. Launch services. Company flyer at 7th European cubesat Symposium 2015.
- [26] JAMSS Team. Process and recent lessons learned of cubesat launch and deployment from japanese experiment module of iss. Technical report, Japan Manned Space Systems Corporation (JAMSS), 2015.
- [27] Jacopo Antichi, Matteo Munari, Demetrio Magrin, and Armando Riccardi. Modeling pyramidal sensors in ray-tracing software by a suitable user-defined surface. *Journal of Astronomical Telescopes, Instruments, and Systems*, 2(2):028001–028001, 2016.
- [28] E. Hecht. *Optics*. Addison-Wesley, 2002.

- [29] ZEISS. Planar t* 1,4/85 technical specifications. Technical report, ZEISS, 2013.
- [30] Carl Zeiss Camera Lens Division. Camera lens news. Technical report, ZEISS, 2009.
- [31] Steve B. Howell. *Handbook of CCD Astronomy*. Cambridge University Press, 2006.
- [32] E. Bendek, R. Belikov, and S. Thomas. Centaur, a scientific and technology pathfinder for direct imaging exoplanets missions. In *Proceedings of the 4th Interplanetary Cubesat Workshop*, 2015.